An outlook on future design of hybrid PET/MRI systems

Zaidi, Habib; Del Guerra, Alberto

How to cite

ZAIDI, Habib, DEL GUERRA, Alberto. An outlook on future design of hybrid PET/MRI systems. In: Medical physics, 2011, vol. 38, n° 10, p. 5667–5689. doi: 10.1118/1.3633909

This publication URL: https://archive-ouverte.unige.ch/unige:23491
Publication DOI: 10.1118/1.3633909

An outlook on future design of hybrid PET/MRI systems

Habib Zaidi[a)]
Division of Nuclear Medicine and Molecular Imaging, Geneva University Hospital, CH-1211 Geneva, Switzerland; Geneva Neuroscience Center, Geneva University, CH-1211 Geneva, Switzerland; and Department of Nuclear Medicine and Molecular Imaging, University Medical Center Gronigen, University of Groningen, 9700 RB Groningen, The Netherlands

Alberto Del Guerra
Department of Physics "E. Fermi," University of Pisa, Largo Bruno Pontecorvo, 3, 56127 Pisa, Italy and Istituto Nazionale di Fisica Nucleare, Sezione di Pisa, 56127 Pisa, Italy

(Received 20 March 2011; revised 12 August 2011; accepted for publication 15 August 2011; published 26 September 2011)

Early diagnosis and therapy increasingly operate at the cellular, molecular, or even at the genetic level. As diagnostic techniques transition from the systems to the molecular level, the role of multimodality molecular imaging becomes increasingly important. Positron emission tomography (PET) and magnetic resonance imaging (MRI) are powerful techniques for *in vivo* molecular imaging. The inability of PET to provide anatomical information is a major limitation of standalone PET systems. Combining PET and CT proved to be clinically relevant and successfully reduced this limitation by providing the anatomical information required for localization of metabolic abnormalities. However, this technology still lacks the excellent soft-tissue contrast provided by MRI. Standalone MRI systems reveal structure and function but cannot provide insight into the physiology and/or the pathology at the molecular level. The combination of PET and MRI, enabling truly simultaneous acquisition, bridges the gap between molecular and systems diagnosis. MRI and PET offer richly complementary functionality and sensitivity; fusion into a combined system offering simultaneous acquisition will capitalize the strengths of each, providing a hybrid technology that is greatly superior to the sum of its parts. A combined PET/MRI system provides both the anatomical and structural description of MRI simultaneously with the quantitative capabilities of PET. In addition, such a system would allow exploiting the power of MR spectroscopy (MRS) to measure the regional biochemical content and to assess the metabolic status or the presence of neoplasia and other diseases in specific tissue areas. This paper briefly summarizes state-of-the-art developments and latest advances in dedicated hybrid PET/MRI instrumentation. Future prospects and potential clinical applications of this technology will also be discussed. [DOI: 10.1118/1.3633909]

Key words: PET/MRI, molecular imaging, hybrid scanner, detectors, attenuation correction

I. INTRODUCTION

The continuous evolution of medicine has led to the necessity of studying biochemical processes at a molecular level for clinical diagnosis and monitoring, pharmacology, genetic and pathological investigations.[1] This field of research is usually called molecular imaging.[2] Among the various molecular imaging techniques, positron emission tomography (PET) is an exquisitely sensitive method for the quantitative investigation of events at the molecular level through the use of radio-labeled tracer molecules and has proved to be one of the most powerful methodologies *in vivo*. The profound success of PET lies in the wide range of biologically relevant probes and results from its high sensitivity for tracer detection (10^{-11}–10^{-12} mol/l),[3] absolute quantification of tracer distribution with good spatial resolution (~4 mm for clinical whole-body systems). Magnetic resonance imaging (MRI) reveals structure and function through the interaction of a strong magnetic field with primarily the protons present in water, fat, etc., and their chemical environment. This modality has also had a profound effect on the practice of medicine and radiological sciences, having a good sensitivity (10^{-3}–10^{-5} mol/l) and an excellent spatial resolution (~1 mm isotropic for clinical systems). It should be noted that the resolution in MRI depends on the signal-to-noise ratio (SNR) and could indeed be better than 1 mm. The wide variety of imaging sequences, along with better soft-tissue contrast compared to x-ray computed tomography (CT), makes MRI an important diagnostic tool. In addition, MRI does not use ionizing radiation and as such has many advantages compared to CT for small-animal imaging, the pediatric population and for applications where radiation dose is a concern.

PET reveals physiology rather than anatomy; the anatomical information provided is either highly variable, depending on the tracer uptake distribution, or it is almost entirely absent for some highly specific tracers. The more specific a tracer is, the higher is the need for anatomical information. Nowadays, there are tracers and tracer systems under development that are very specific. The inability of PET to provide anatomical information is a major limitation of PET-only studies and consequently, it has been recognized that to

maximize the potential of PET, this technique needs to be combined with an anatomical imaging modality, such as x-ray CT or MRI. Adding anatomical information allows accurate localization of the PET signal and also facilitates improvement in the quantitative accuracy of the PET signal through correction of the error in quantification that results from the finite spatial resolution of PET (partial volume effect).[4,5] These benefits have resulted in software approaches to coregister PET images to those from CT or MRI,[6] which generally work rather well in the brain but not in the thorax and abdomen where there is nonrigid motion between the two scans, and although transmission scans are available for software coregistration, these too exhibit poor anatomical detail. The development of combined PET/CT scanners for preclinical and clinical imaging has made possible acquisition of both structural and functional images.[7,8] Even though CT has certain advantages in oncological imaging, a highly attractive alternative to PET/CT is to combine PET with MRI, since the repertoire of MR examinations is highly complementary to PET.[9]

PET and MRI are powerful imaging techniques used in a wide spectrum of research applications, ranging from process engineering, biomedical research, and clinical diagnostics. Utilization of fusion imaging combining PET and MR is expected to grow as more molecular targeted imaging agents are being developed. Today, there are more than 29 000 PubMed entries since 1980 (about half of them published during the last 5 years) when searching for "*PET*," "*MRI*," and "*FUSION*" (Fig. 1). It should be noted that this search does not imply that there are 29 000 papers dealing with PET/MRI fusion or integration, but only that the increase of the occurrence of these words is an indicator of the rapidly growing field (an increase of ~150% from 2005 to 2010).

In response to the requirements of multimodality imaging, several investigators proposed and are developing various approaches specifically designed for clinical imaging that allow one to combine through hardware approaches, the power of PET with other imaging modalities such as x-ray CT,[10] MRI,[11] and optical imaging (OI).[12] Although multimodality systems such as single-photon emission computed tomography (SPECT)/CT and PET/CT have been successfully implemented in the clinic,[10,13] the combination of PET and MRI still represents the frontier challenge for molecular imaging technology.[11] Conventional PET systems employ photomultiplier tubes (PMTs) to detect the scintillation light. However, PMTs are sensitive to magnetic fields and, therefore, cannot be operated inside an MR system. Several approaches have been investigated in order to overcome this problem, such as the use of light guides to take the scintillation light out of the MR system, where the PMTs can be properly operated, or the use of avalanche photodiodes (APDs) that are insensitive to magnetic fields. More recently APDs working in Geiger mode (GM-APD), also known as silicon photomultipliers (SiPMs), have been proposed.[14] All of these solutions have limitations and several academic research groups, and companies are working on various prototypes of combined PET/MRI systems.

Nevertheless, despite the difficulties and known limitations, several design approaches have been proposed and used in clinical setting. The number of scientific contributions related to this subject has been increasing steadily during the last decade, which motivated the writing of this paper as a snapshot of the dynamically changing field of combined PET/MRI instrumentation.[15] A detailed description of the various approaches proposed in the literature is given. We also discuss some important considerations and limitations of systems proposed so far. The strategies followed for clinical validation of novel technologies are briefly described. Future opportunities and the challenges facing the adoption of hybrid PET/MRI systems and their role in basic and clinical research will be addressed as well.

II. HISTORICAL DEVELOPMENT OF PET/MRI

The interest in PET scanning within strong static magnetic fields was first suggested by the need to reduce the distance positrons travel before annihilation (positron range) through magnetic confinement of the emitted positrons.[16–19]

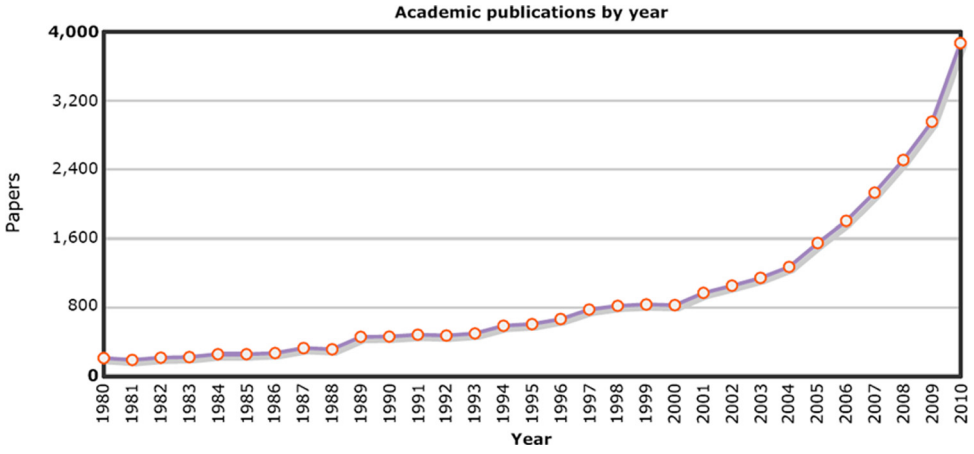

FIG. 1. The increasing number of annual peer-reviewed publications reporting on the use of PET/MR fusion demonstrates the growing interest in combined PET/MR. This graph is based on a PubMed query with using the following mesh terms: "PET" OR "POSITRON EMISSION TOMOGRAPHY" AND "MRI" OR "MAGNETIC RESONANCE IMAGING" AND "FUSION" OR "REGISTRATION". A time line was created with MEDSUM: an online MEDLINE summary tool by Galsworthy, MJ. Hosted by the Institute of Biomedical Informatics (IBMI), Faculty of Medicine, University of Ljubljana, Slovenia (Ref. 206).

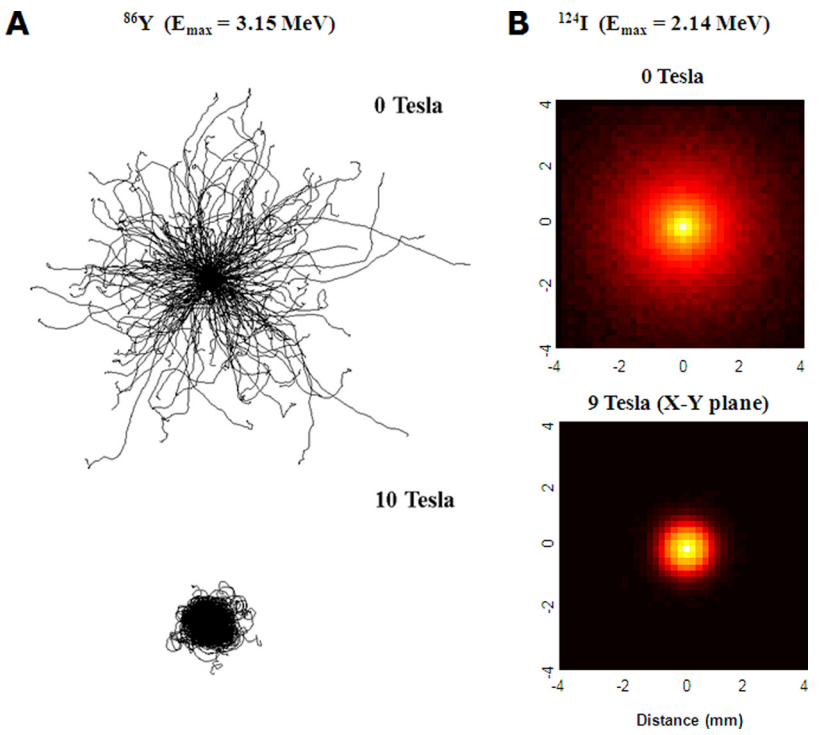

FIG. 2. (a). Influence of the magnetic field on positron range, for ^{86}Y ($E_{max} = 3.15$ MeV) in water, illustrated by Monte Carlo simulations obtained at 0 T (top) and 10 T (bottom) field. The 3D tracks are projected onto a plane perpendicular to the direction of the magnetic field. The average distance between the emission and annihilation point is reduced considerably in the presence of the magnetic field. (b). Simulated positron range reduction for I-124 ($E_{max} = 2.14$ MeV) in a 0 T (top) and 9 T (bottom) magnetic field. Adapted with permission from Blanco *et al.*, Nucl. Phys. B, Proc. Suppl., **158**, 157–160, 2006 and Burdette *et al.*, *IEEE Nuclear Science Symposium Conference Record*, 2376–2380, 2005. Refs. 20, 22.

A magnetic field collinear with the axis of the scanner will improve its transaxial resolution, since the positron range is reduced in that plane, while keeping the axial resolution unaltered.[19,20] Indeed, Monte Carlo simulation studies predicted improvements in spatial resolution for high energy positron emitters ranging between 18.5% (2.73 mm instead of 3.35 mm) for ^{68}Ga and 26.8% (2.68 mm instead of 3.66 mm) for ^{82}Rb for a magnetic field strength of 7 T.[21] Figure 2 shows the compression of the spatial extent of positron trajectories originating from a spectrum with maximum energy of 3.15 MeV (^{86}Y) and 2.14 MeV (^{124}I) in a magnetic field of 10 and 9 T, respectively, obtained using Monte Carlo simulations.[20,22]

It is amazing to point out that the history of combined PET/MRI dates back to the mid 1990s even before the advent of PET/CT.[23] Early attempts to design MR-compatible PET units relied on slight modification of PET detector blocks of a preclinical PET scanner to keep the PMTs at a reasonable distance from the strong magnetic field of a clinical MRI unit.[24] To avoid mutual interference between both systems, the detectors were coupled to long optical fibers (4–5 m) to bring the light from the scintillator to the photomultipliers and read-out electronics outside of the magnetic field, leading the weak scintillation light outside the fringe magnetic field to position-sensitive PMTs.[25,26] One major drawback of this design is that the long fibers result in the loss of a significant fraction of the scintillation light, thus affecting the energy and timing resolution, deteriorating crystal identification and losing PET signal performance, thus impairing the overall PET performance.

Despite the limitations of this design, similar approaches were adopted by other investigators.[27–31] Other related design concepts based on conventional PMT-based PET detectors rely on more complex magnet designs, including a split-magnet[32] or a field-cycled MRI.[33] In the former design, an 8 cm gap in the axial direction of the B_0-field of a 1 T actively shielded superconducting magnet houses the preclinical PET scanner and shorter (1.2 m long) optical fiber bundles.[32,34] This allows to place the PMTs at very low-field strength (~30 mT). The major advantage of this design is that only minor modifications of existing conventional PET detectors are required, still the magnet and gradient coil design are more complex and expensive compared to the technologies used on typical MRI scanners. In the latter approach, the PMTs are built into the magnet, but PET scanning is allowed only within small time intervals (~2.5 s) when the MR polarizing and read-out fields are switched off.[33,35] The switching cycle for the 1 T polarizing field requires about 1 s to magnetize the object and is shut-down very quickly. The hardware implementation of this design still needs to be demonstrated given that the exposure of the PMTs to a variable magnetic field remains challenging. In addition, the use of electromagnets (instead of superconducting magnets) for field-cycled MRI engages significant compromises.

The potential of novel read-out technologies insensitive to magnetic fields including APDs and SiPMs was yet realized to reach this endeavor. APD-based technology is already successfully implemented by one small-animal PET vendor[36] and on many preclinical[37–41] and dedicated breast[42] PET/MRI systems. SiPMs, small finely pixelated APDs operated in "Geiger mode," and more recently the Digital SiPMS,[43,44] have a large potential for further improvement; however, their current performance (high gain and an excellent SNR) is sufficiently good to be considered strong candidates for the design of combined PET/MRI scanners[43–46] since they allow to reduce significantly the amount of electronics needed inside the MRI.[47] SiPMs are, currently, commercially available from several vendors.[48] The development of combined

PET/MRI based on APDs is one of the promising designs achieved so far. The first *in vivo* mice images confirmed the capability of the system for performing simultaneous PET/MR imaging.[39,41] Further experimental analysis showed that both systems work with unhindered performance, consolidating the observation that each modality is virtually invisible to the other.

The conceptual design of combined PET/MRI instrumentation for humans benefited to a great extent from experience gained in preclinical imaging. The promising results obtained on preclinical systems encouraged one of the major industrial leading players (Siemens Healthcare) to develop the first clinical PET/MRI prototype (BrainPET) dedicated for simultaneous brain imaging in collaboration with the University of Tuebingen, Germany.[49,50] The system was assessed during the last 3 years in a clinical setting by exploiting the full potential of anatomical MRI in terms of high soft-tissue contrast sensitivity in addition to the many other possibilities offered by this modality including BOLD imaging, functional MRI (fMRI), diffusion-weighted imaging (DWI), perfusion-weighted imaging (PWI), and diffusion tensor imaging (DTI).[51,52] A second, in this case sequential combined PET/MRI system, was also designed for molecular-genetic brain imaging by docking separate PET and MR systems together so that they share a common bed, which passes through the field-of-view of both cameras.[53] This is achieved by combining two high-end imaging devices, namely the high resolution research tomograph (HRRT) and a 7 T MRI with submillimeter resolution.

On the other hand, the prospective applications of a whole-body PET/MRI system have been explored in the literature.[54–72] Such a system would allow exploiting, in addition to the above discussed applications, the power of MR spectroscopy (MRS) to measure the regional biochemical content and to assess the metabolic status or the presence of neoplasia and other diseases in specific tissue areas. Until concurrent PET/MRI technologies for whole-body imaging become more mature and economically viable, other approaches for so-called sequential PET/MR imaging have been researched.[73] One such system is the Philips Ingenuity TF PET/MRI, a hybrid imaging system with Philips time-of-flight GEMINI TF PET and Achieva 3 T X-series MRI system.[74] While this design does not allow simultaneous PET and MRI acquisition, it allows acquisition of automatically coregistered PET and MR images acquired sequentially, similar to the workflow in PET/CT systems. Following initial development, two PET/MRI systems were installed in Mount Sinai Medical Center, NY and Geneva University Hospital, Switzerland, while the third was more recently installed at the Forschungszentrum *Dresden*-Rossendorf (FZD) in Dresden, Germany. Performance of the PET subsystem measured using the NEMA NU2-2007 protocol was comparable to the commercial GEMINI TF PET/CT system using phantom and clinical studies.[75] Following the design principles of the dedicated brain PET/MRI, the first simultaneous whole-body PET/MRI system called Biograph mMR was developed by Siemens Medical Solution and installed recently at University of Munich, Eberhard Karls University Tuebingen, and the Fiedrich-Alexander-University in Erlangen, Germany. Another system is being installed at Massachusetts General Hospital in Boston. More recent developments of PET/MRI instrumentation are discussed in Secs. III A and III B.

III. DESIGN CONSIDERATIONS OF PET/MRI SYSTEMS

Clearly, the soft-tissue contrast of MR provides a superb anatomical reference for the molecular PET data, but MR can also provide significant functional data of its own, such as diffusion-weighted MR for assessing tissue ischemia, contrast-based perfusion measurements in the brain and heart, fMRI and angiography. The ability to simultaneously acquire MR and PET data would provide simultaneous PET and MR functional measurements, of particular interest in the brain, and would circumvent the coregistration errors induced by organ movement during transfer from one scanner to the other. There is considerable added value from a simultaneous PET/MRI system, since we can consider using real-time MR data to rebin the PET data to account for organ motion.[76] Additionally, MR data can be used to guide statistical approaches to PET image reconstruction using MR-derived prior functions.[77,78] Furthermore, the axial magnetic fields employed in MR reduces the positron range in the transaxial plane resulting in an improvement of the spatial resolution of the PET scanner.[16–19] It should be emphasized that this is not noticeable at currently implemented field strengths of 2.8 T (Siemens Healthcare) and 3 T (Philips Healthcare).

There are several ways to combine PET and MRI imaging of the same patient.[73,79] The simplest one is to adopt the same arrangement as for PET/CT, in the so-called "tandem" configuration [Fig. 3(a)], where the two examinations are taken sequentially in space and time. However, a very attractive solution is to have the MRI and PET examinations taken simultaneously in space and possibly in time. This solution has brought to the "insert" concept [Fig. 3(b)], where a small axial size PET insert fits inside a standard MRI scanner, and to the "fully integrated" version [Fig. 3(c)], where a dedicated whole-body PET scanner is built in a dedicated MRI scanner. This latter solution is the most challenging one, but it is certainly the one that can bring to a real step forward the use of combined PET/MRI systems in diagnosis, therapy, and follow-up.[11]

The main issue for combining PET and MR imaging modalities in a single device is to avoid degradation of the performance of either scanner. All existing approaches involve some compromises in performance such as reduced PET sensitivity and quantification capability and MR gradient performance. The goal of the many research groups working in this field is to develop an innovative fully MR compatible detector module with a flexible design that can be employed in PET applications outperforming current scanners.

The seamless integration of PET and MR also requires significant software development: Monte Carlo simulations to determine the final design of the detector module and to optimize it for PET applications;[73] dedicated image reconstruction

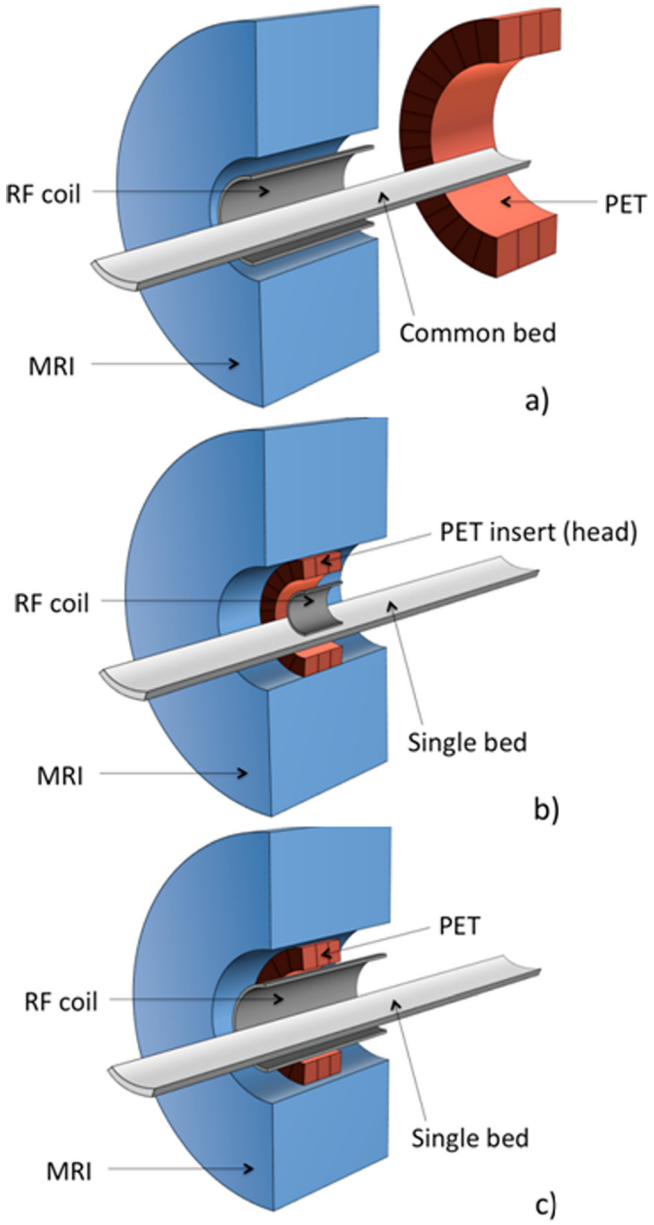

FIG. 3. Artistic cross-view of various potential designs of combined PET/MRI systems: (a) tandem: The two scanners are mounted together back-to-back allowing sequential (like PET/CT) rather than simultaneous acquisition, (b) insert: The PET scanner is inserted between the RF-coil and gradient set of the MR system, (c) full integration: the two systems are fully integrated within the same gantry.

using fully 3D statistical based algorithms;[78] simulations and analytical models to generate the appropriate system response matrix to be included in the reconstruction algorithm.[80,81] In addition, time-of-flight (TOF) techniques need to be used in clinical applications, especially for whole body, for instance, by including the TOF information in the image reconstruction. Because TOF PET technique should be also implemented, fast scintillators and very fast photodetectors must be used. New scintillators such as LSO codoped with calcium (LSO:Ce,Ca), that has a decay time of 30 ns instead of 40 ns of LSO:Ce, improved light yield and reduced afterglow[82] seems a promising solution. The advantages of TOF for clinical whole-body PET are well demonstrated.[83–87] The difference in the arrival time between the two detectors in coincidence can be used to reduce the uncertainty in the annihilation point of the event to a limited region along the line of response, and thus to diminish the noise in the reconstructed images. A timing resolution of 500 ps results in a reduction of a factor of 5 in the variance of the reconstructed image compared to conventional PET.[88] The development of ad-hoc techniques aimed at compensating or correcting for image degradation effects and at ensuring quantitative information, such as normalization, scatter, attenuation, etc., are also necessary.

In the following two sections, we will illustrate in detail the three approaches for combined PET/MRI systems and discuss their advantages and drawbacks.

III.A. Instrumentation for sequential PET/MR imaging

The simplest method to obtain combined PET/MR images is to use the so-called tandem configuration, where MRI and PET are taken sequentially one after the other in two separate scanners. This could be achieved by having both systems in the same room or in separate rooms. The later design was adopted by General Electric Healthcare and installed at Zurich University Hospital. The same patient transfer table top (PTTT) is docked on the two imaging modality gantries and used for both PET/CT and MR examinations. The second sequential design concept makes use of the same bed for the patient for a tandem configuration of PET and MR systems within the same room [Fig. 3(a)]. This is also the cheapest solution from an economic point of view because the only technological improvement is the additional shielding for the MR magnetic field, so as to have a negligible effect on the nearby PET performance,[89] and the necessity of having a patient bed in cosharing among the two scanners.

Such a solution has been recently implemented by Philips Healthcare that has made commercially available an MRI scanner in the same suite as a PET camera, called Ingenuity TF PET/MRI.[75] The two scanners are placed about 4.2 m apart (distance between centers of FOV), with a patient table located in between that can pivot 180° to allow patients to be shuttled from one scanner to the other without getting off the table (Fig. 4).

The advantages of this solution are mainly in the reduced cost, marginally above the cost of the two single scanners, the lack of additional claustrophobia because of the large separation between the two scanners and the simplicity of image coregistration. Another important advantage is that the high level of quantification and image quality of a TF PET/CT and an unaffected MR could be used. However, the lack of simultaneity of the two modalities introduces organ motion effects and prevents the possibility of highly precise quantitative measurements and, most of all, of functional PET-functional MRI simultaneous investigations. Another limitation is related to the room size needed for the installation of sequential PET/MRI systems since they need larger room than standard PET/CT or integrated PET/MRI systems. The typical room size required for such a system including technical space is 4.3×13 m.

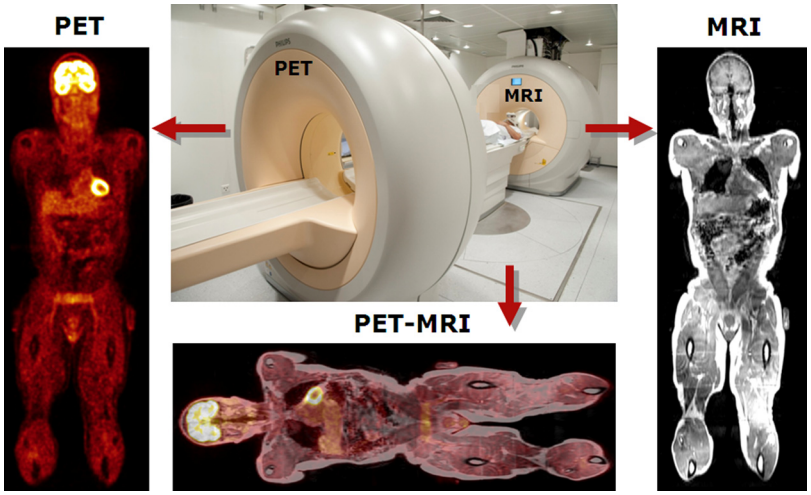

FIG. 4. Photograph of the Philips whole-body Ingenuity TF PETMR system design installed at Geneva University Hospital. A turntable patient handling system facilitates patient motion between the Achieva X-series 3 T MRI system on the left and the time-of-flight PET system on the right. Whole-body MRI, PET, and fused PET/MRI images area also shown.

III.B. Instrumentation for concurrent PET/MR imaging

The combination of the two modalities in a single instrument imposes severe technical challenges. The development of a PET scanner that can be operated in combination with an MR scanner must overcome two main limitations, namely the space constraint inside the magnet and the interference between the two modalities. This imposes the use of photodetectors that are insensitive to magnetic fields and read-out electronics with minimum heat radiation. On the other hand, the effect of the PET detector on the performance of the MR scanner, due to the PET electronic interference on the RF and gradient coils, especially if high frequency digital clocks are used for read-out electronics or if eddy currents are produced, must be minimized.[90,91] Additionally, the intrinsic performance on both modalities should be at least similar to what can be achieved on state-of-the-art scanners. The latest measurements on the mMR show that the interference of the PET on the MR is practically negligible.[92]

As discussed in Sec. II, the first solution adopted to minimize the interference was to position the scintillator for the two 511 keV photons detection inside the MRI scanner. In the original design by Christensen *et al.*,[23] the photomultipliers used as photodetectors were replaced by Position sensitive avalanche photodiodes (PAPDs) placed at up to 5 m away from the scintillator by Catana *et al.*[37] However, the need to bring the light outside of the magnetic field region puts stringent topological constraints, basically limiting the axial field-of-view that is possible to cover in PET mode with this solution.

III.B.1. Split-field magnet

A similar PMT-based approach to PET/MRI is being pursued by Lucas *et al.*[32] who make use of a novel split-magnet low-field MRI system, which allows a relatively large number of PET detectors to be placed inside the gap within the MRI system and also reduces the fiber length compared with previous systems (Fig. 5). The adopted magnet is a 1 T actively shielded superconducting magnet with a 'split' region where to accommodate a multiring PET detector based on a microPET® focus 120 system (Siemens Molecular Imaging Preclinical Solutions, Knoxville).

By means of 120 cm long fiber, the light is brought to PMTs that are located in 10 gauss (1 mT) field that produces a minimal effect on image quality. On the other hand, the effects of the long fibers on PET performance have been studied by several groups[23,24] that have proved to cause a degradation of detector sensitivity, energy-, timing-, and spatial-resolution. A comparison of the experimental results

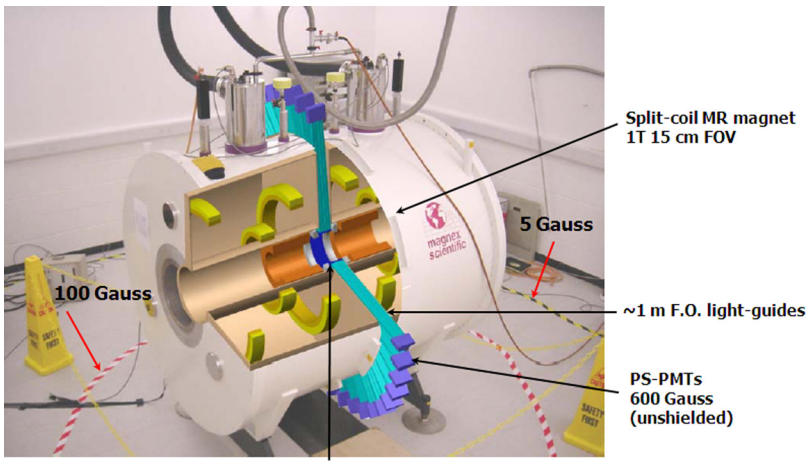

FIG. 5. Schematic of PET/MR system with split-magnet. The cut-away shows scintillating crystal ring (dark grey), fiber bundles (light grey), and screened PMTs (dark grey outside magnet cryostat) and "split" gradient coil (grey). Reprinted with permission from Lucas *et al.*, Technol. Cancer Res. Treat. **5**, 337–341 (2006) (Ref. 32).

between the long (120 cm) fibers and 10 cm short ones showed a degradation of the energy resolution at the photopeak from 17.2% to 27.1% (with a light loss of about 40% for the long fibers), of the time resolution from 2.6 to 3.6 ns, but a negligible sensitivity loss. More noticeably, although the position map on the PMT was deteriorated, it was still good enough to obtain the same spatial resolution (about 1.6 mm).[32] This approach has the major drawback that it requires a special and lower field magnet but has the advantage of excellent decoupling of electronic cross talk between the two modalities. In fact, no interference between the PET system and the pulsed RF, and gradient was observed.[32]

III.B.2. PET insert

A second approach exploits the potential of solid-state light detectors (APDs) to allow the development of an MR-compatible PET detector insert that can be used inside a standard MR scanner [Fig. 3(b)]. The prospect of such an integration of MR and PET has been the subject of several reports in the scientific literature[11,37–42,49,93–100] especially toward animal imaging[101] and grant funded activity.

APD-based PET "insert" systems for conventional small-animal MR systems have been used to acquire the first simultaneous PET/MR images.[37] Those insert systems for small-animal imaging have PET detector rings with small (~60 mm) diameters. This approach to constructing a PET insert system for a conventional MR system results in a small diameter PET detector ring due to the space occupied by the conventional MR gradients. For example, the standard gradient set for a 200 mm bore magnet reduces clear bore access from 200 to 120 mm. The latest version of the PET/MRI system developed at the University of Tuebingen (Fig. 6), following major improvements of the initial design,[38] consists of detector modules comprising a 12×12 LSO scintillator array ($1.6 \times 1.6 \times 4.5$ mm^3), a 3×3 APD array, and custom charge sensitive preamplifier electronics, located within a thin copper shielded housing.[39,41] The multiring PET scanner comprises a total of 10 LSO-APD detector modules with an axial and transaxial FoV of 19 and 40 mm, respectively, to produce 23 slices with a slice thickness of ~0.8 mm.

This approach is also employed in the first prototype of a clinical PET/MRI scanner for head only imaging developed by Siemens Healthcare.[49] The concept has proven to work, and the first studies are ongoing in both preclinical and brain scanner prototypes installed at a limited number of clinical sites.[50] However, the systems still suffer some difficulties in their operation and are far from a stable system that can be commercialized. In addition, these APD-based systems have a comparatively poor timing resolution that makes them incompatible with time-of-flight technique.[102]

This approach is particularly sensitive to degradation of PET performance as a result of the PET electronics suffering interference from both the RF and gradient pulses of the MR scanner.[101] Unfortunately a small increase in magnet radius results in a large increase in magnet cost; furthermore, the strength and efficiency of gradient sets reduce dramatically as the radius of the inner diameter of the gradient increases. On the other hand, the combined gradient set—PET scanner can be used in commercially available magnets for a small-animal MRI, without affecting the cost of the magnet.

III.B.3 Fully integrated PET/MRI scanner

A new solution has been proposed to design a fully integrated hybrid system where a PET scanner and an MRI

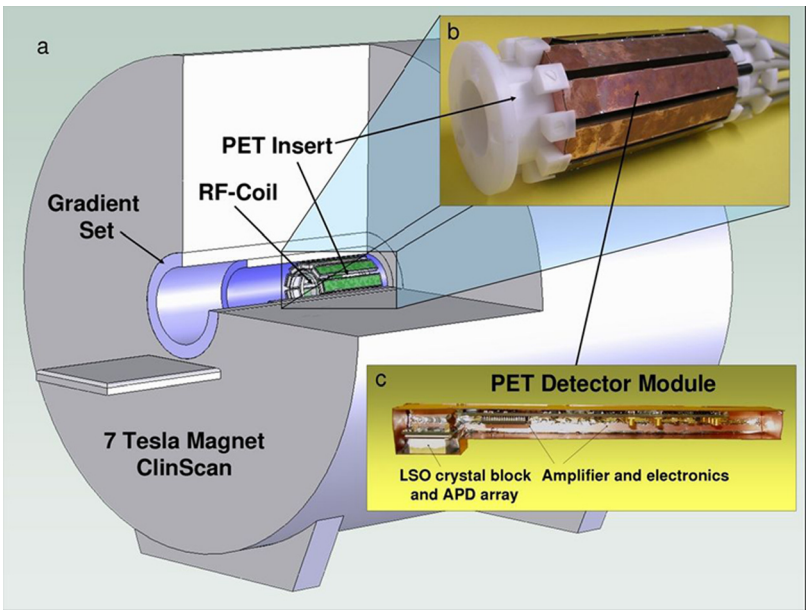

FIG. 6. Combined small-animal PET/MRI developed by the University of Tuebingen (Germany). The PET insert is fully integrated into a 7 T MRI system (ClinScan, Bruker). (a) Drawing of PET/MRI combination, showing the PET insert placed inside the MRI scanner, matching the centers of both fields of view. (b) Photograph of the MRI compatible PET insert, consisting of ten detector modules. (c) Single PET detector module showing the LSO scintillator block, APD-array, and preamplifier built into a MRI compatible copper shielding. The system showed excellent performance without noticeable mutual interference between the two modalities. Reprinted with permission from Judenhofer *et al*., Nat. Med., **14**, 4, 459–465, 2008 (Ref. 41).

scanner are combined in a single device [Fig. 3(c)]. It has been reported that significant system interaction occurs when inserting PET detector electronic components into the gradient and RF coils in an existing MR system.[101] The PET electronics might impact the signal-to-noise achievable with the MR system, however, the MR operating frequency band is relatively narrow and not necessarily affected by interference from the PET electronics. Also to prevent gradient and RF pulses being picked up by the PET electronics, walled screens of 0.15 mm copper have been introduced to provide adequate electromagnetic attenuation, which then results in a degradation of MR pulse performance with an SNR reduction of about 30%.[38] Unless the shims, gradients and RF transmitter are designed as an integral whole, optimal performance might be compromised and will be tricky to achieve and maintain.

Hence, the instrumentation requirements for the next generation 4D high performance PET detector module compatible with the MR environment are very challenging. The MR compatible PET module will have to provide highly accurate 3D position information and fast timing information, while having at the same time a high intrinsic efficiency. It is conceivable that the module design will be based on the use of matrices of pixilated crystal or continuous scintillator crystals in combination with fast, novel photodetectors of high granularity.

III.B.4. Detector modules for integrated PET/MRI scanners

The recent advances in front-end electronics and computing technology and the increasing need for multimodality instrumentation such as PET/MRI now opens new opportunities for the advent of novel kinds of detectors. A key feature for the success of the integrated PET/MRI scanners is the use of multicell Geiger-mode avalanche photodiodes (GM-APD), also known as silicon photomultipliers (SiPMs), for light detection which allow the exploitation of integrated design features that minimize interference between the two modalities and, hence, preserve PET and MR performance. The SiPM is a novel type of photodetector that has had a rapid development and has reached a performance level that can offer significant improvements in medical imaging applications.[103–107]

A SiPM pixel is a matrix of the GM-APDs (microcells) connected in parallel by means of a resistive layer. In this way, they permit to accurately measure the energy deposited for a moderate photon flux ($N_{\text{photons}} < N_{\text{microcells}}$). They are small, light and insensitive to magnetic fields. Different geometries such as square devices of 1×1, 2×2, 3×3, and 4×4 mm^2, circular devices, and 1D and 2D arrays, have been implemented to fulfill the requirements of several different applications [Fig. 7(a)]. In addition, their improved characteristics in comparison to other solid-state photodetectors (e.g., APD), namely high gain and excellent SNR, timing resolution, together with their potential for further development and optimization for different applications, make SiPMs the best candidates to be employed as photodetectors in PET and PET/MRI. In order to handle the low gain of the APD, a low input noise charge amplifier is usually adopted. Because of the intrinsic variation of the gain of the APD with temperature, the time resolution is strongly limited due to the variation of the time jitter. A recent ASIC-based system has achieved a time resolution of 5.4 ns with LYSO crystal.[102] Although the percentage gain variation with temperature of the SiPM is basically the same as for the APD, the very fast intrinsic rise time (below 100 ps) of the SiPM signal makes this device an extremely good candidate for TOF-PET[84,85]

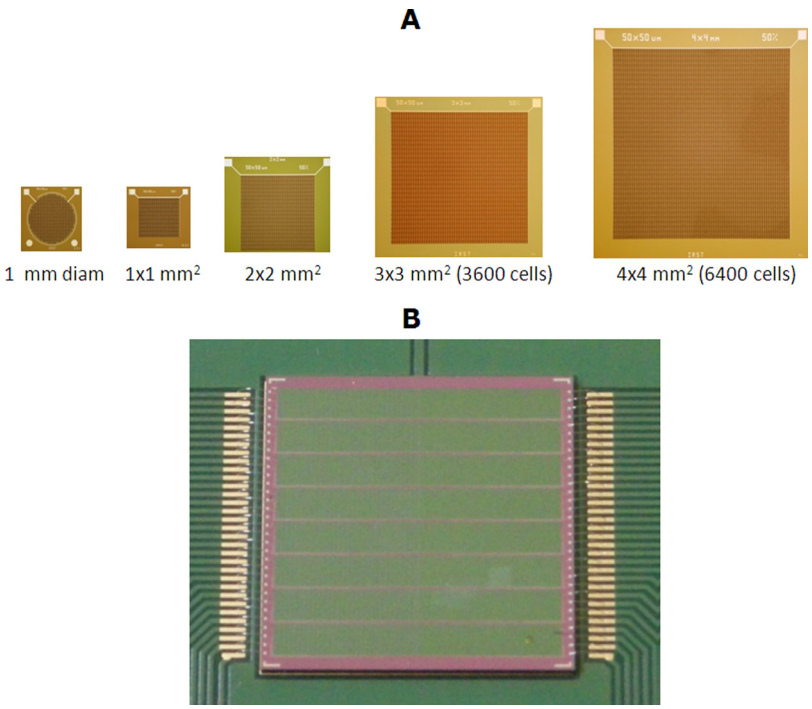

FIG 7. (a) Photograph of various sizes of SiPM samples. (b). Photograph of the 8×8 matrix of 1.5 mm $\times$ 1.5 mm pixel with lateral read-out from two sides only, as developed by FBK-irst (Trento, Italy). Adapted with permission from Llosa *et al.*, Phys. Med. Biol., **55**, 23, 7299–7315, 2010 (Ref. 207).

and PET-MRI systems with TOF capability. On the other hand, it is not only the rise time of the SiPMs that defines the pulse length of the system scintillator-SiPM which is an important parameter for energy resolution and dead time limitation. In fact, the decay time is very relevant since the system output is the result of the convolution of the LYSO response with the SiPM response. Single-photon spectra and energy spectra for 511 keV photons have been acquired, while the SiPMs are in the magnetic field and MR gradients and radiofrequency (RF) pulses are driven. The results clearly demonstrated that the performance of these photodetectors are not affected either by static magnetic field or by gradient switching.[108] It should be noted that in most of the cases, it is not only the device itself but also the circuit that interfaces the device that leads to noticeable interference.

Silicon photomultipliers from different manufacturers are now commercially available, with different sizes, geometries, and photodetection characteristics based on different detector layouts. Matrices of SiPMs are built by means of individual SiPM embedded in a mechanical support with a reasonable small dead space and are available in centimeters (and more) side assembly. Monolithic matrices [Fig. 7(b)] with a minimal dead area between the SiPM pixel elements have been built by FBK-irst (Fondazione Bruno Kessler, Trento, Italy), with excellent performance characteristics and high production yield.[109–111]

In the case of preclinical applications, a granularity of 1.5 mm × 1.5 mm has been suggested for the photodetector. Simulations based on this configuration predict an intrinsic spatial resolution of 0.4 mm full width at half-maximum (FWHM) around the center of the crystal, which, however, degrades toward the detector edges. The predictable spatial resolution for a preclinical PET scanner with a ring diameter of 10 cm based on this detector module is below 1 mm for an F-18 source in the center of the FOV using the filtered backprojection algorithm.[47,110] For whole-body applications, a photodetector pitch of 3 mm × 3 mm or larger is probably adequate, aiming at a spatial resolution of about 2 mm.

III.B.5. Dedicated ASIC and data acquisition read-out electronics

Given the high granularity of the photodetectors, the use of a dedicated front-end ASIC is mandatory to meet the photodetector and scintillator characteristics. In fact, it is not possible to have off-the-shelf electronics or even semicustom read-out. The number of channels for a PET tomograph can easily reach 20–40k channels and an integrated solution must be implemented. Furthermore, the read-out system has also to be adapted to the photodetector-scintillator package performance, aiming at preserving the intrinsic fast response of the SiPM.[112] In fact, in clinical applications a fast response of the front-end electronics is essential to implement the TOF technique. A fast read-out system is also necessary to reduce noise and event pileup, in particular, in preclinical applications in which the count rate per unit area is higher. Many research groups are working on ASIC development specifically designed for reading SiPM-scintillator detectors, in particular for PET applications. Among these it is worth mentioning the Orsay group, that has originally developed an ASIC called MAROC suitable for the position-sensitive PMT,[113] that was successfully adapted to the read-out of SiPM matrices[114] and a specific ASIC for SiPM, called SPIROC.[115] A position-sensitive time ASIC (PETA) was developed by the Heidelberg group, specifically for large-scale PET applications.[116] It also performs a programmable integration, and time stamping and digitization. A multi-University Italian collaboration has developed a specific ASIC,[117] called BASIC,[118] initially an 8-channel, now a 32-channel,[119] coupled to a dedicated fast electronic read-out based on FPGA. The main features of the ASIC are that it is based on a current amplifier, the output of which is duplicated by current mirrors, so as to allow simultaneous high time resolution and energy measurement. The two signals are shaped by a fast and slow shaper, respectively. Preliminary results for two LSO:Ce,Ca crystal read-out by two SiPMs through the entire read-out chain shows a coincidence time resolution of 185 ps (σ) (Fig. 8).[120] This excellent result assumes 1:1 coupling with the crystal pixel.

An essential issue when working with SiPMs is the variation of the breakdown voltage with temperature, which results in gain and photodetection efficiency (PDE) variations.[121] This is even more important in an MR compatible system, owing to the strong temperature variations in the confined magnet environment, that requires calibration tests, monitoring, and temperature control of the whole detector. In addition, eddy currents induced by the gradient system in the conducting structures of the PET housing can result in a local increase of the temperature in some regions. The use of an ASIC in a PET/MRI environment thus requires a special additional caution in terms of limiting the power consumption for the ASIC, so as to reduce the stringent temperature control requirements.

The high number of channels necessary for read-out of the proposed module is possible with current fast, high performance ASICs and electronics. However, special considerations are needed to operate the module inside an MR scanner to avoid interference between the two systems. Switching signals, such as clocks, can easily interfere with the MR detection and, therefore, analog-to-digital conversion of the signals must be performed far from the MR receiver coil. A possible solution is the use of optical fibers to convey the detector analog signals, multiplexed by the ASIC, with the aid of some control signals, outside the MR detectors where they will be digitized. Optical fibers are ideal candidates for signal transmission within the MR detector, and several fibers may be bundled together, thus reducing the physical space and labor requirement, while providing the same bandwidth capacity of a multifiber cable with individual fiber/connector terminations per fiber.

III.B.6. Digital SiPM

The standard SiPM is essentially an analog device with a linearity that depends upon its intrinsic granularity and number of microcells. PET instrumentation is going more and

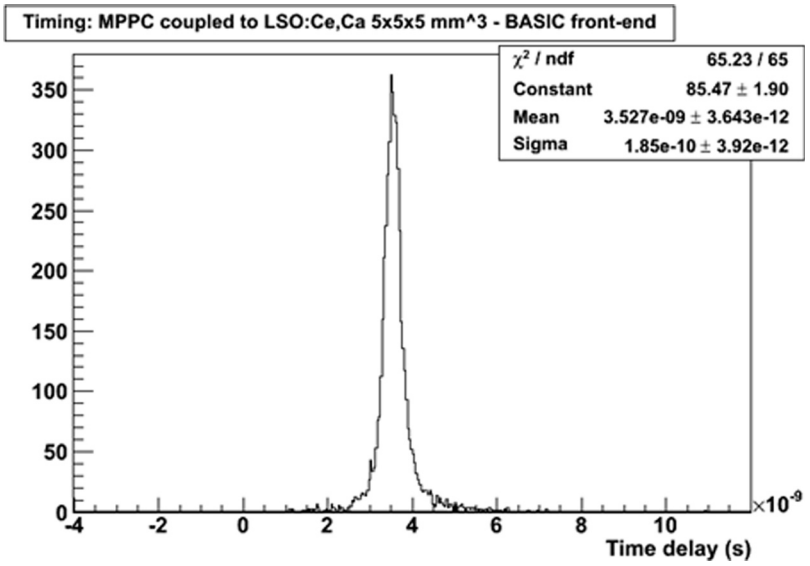

FIG. 8. Time delay distribution of two 3×3 mm^2 SiPMs (multi-pixel photon counters (MPPCs) manufactured by Hamamatsu) coupled to a $5 \times 5 \times 5$ mm^3 LSO:Ce,Ca crystal each, read-out by two BASIC chips in time coincidence. Reprinted with permission from Marcatili *et al.*, Nucl. Instr. Method A, 2011 (in press) (Ref. 120).

more toward the direction of a fully digital read-out and handling of the data, and even more so with the proposed PET/MRI systems. In this respect, it would be very convenient to have a solid-state detector, whose response is intrinsically digital without going through dedicated read-out, amplifier ASICs, ADCs, etc. This ambitious idea has been recently concretized with the first example of a "fully digital SiPM" (dSiPM).[43,44] This sensor is based on a single photon avalanche photodiode (SPAD) integrated in a standard CMOS process. The block also contains active quenching and recharge circuits as well as a one bit memory for the selective inhibit of detector cells. The trigger signal from all cells is transported to the integrated time-to-digital converter (TDC). Photons are detected and counted as digital signals. This device (dSiPM) has a size of 3.8 mm × 3.3 mm containing 8188 individual Geiger-mode cells. The coincidence timing resolution using a ^{22}Na source for 3 mm × 3 mm × 5 mm LYSO crystals coupled to these dSiPM was 153 ps FWHM. The energy resolution at 511 keV was 10.7% FWHM for 4 mm × 4 mm × 22 mm crystals.[44] Also, SiPM sensor tiles with 8×8 channels controlled by an FPGA interface board have been recently reported.[122]

More development of similar devices in CMOS technology is expected and will certainly be of great benefit for PET/MRI systems.

III.B.7. Latest advances

Along these lines a new project for combined full-body PET/MR imaging with silicon photomultipliers and pixilated crystals, the HYPERImage project[123] has started in 2008 (FP7/2007-2013). This project is funded by the European Commission under the first Health call of the FP7 and coordinated by Philips Research. The use of a split-coil (gradient) offers the advantage that the gap can be made large enough to accommodate a PET detector of increased dimensions, both axial and transaxial, resulting in a FOV similar to the state-of-the-art commercial devices. More recently, the SUBLIMA project lead by Philips Technologie GmbH was funded by EU-FP7 in 2010.[124] The project aims at truly simultaneous, fully integrated, solid-state PET/MRI technology for concurrent functional and anatomical imaging.

On the other hand, and as discussed in Sec. II, the first whole-body PET/MRI prototype (mMR) was recently developed by Siemens Healthcare and is now being assessed in clinical setting (Fig. 9). The detector block consists of 8×8 LSO crystals read-out by a matrix of 3×3 APDs. The MR system uses the TrueForm magnet design to provide improved MR image quality even at the edges of the field of view (FOV), improved spectral fat saturation and less overlap is needed for multistation (multiple bed) acquisitions. The transaxial FOV of the MR is 50 cm, whereas the axial FOV is 45 cm. The PET subsystem consists of 8 rings of 56 blocks with an axial FOV of 25.8 cm and ring diameter of 65.6 cm. It is worth noting that the MR scanner is specially designed for the Biograph mMR and fully integrated with the PET architecture. Some preliminary results achieved using this system were presented at the 2011 meeting of the Society of Nuclear Medicine.[92,125]

IV. MR USAGE FOR QUANTITATIVE IMAGING ON HYBRID PET/MRI SYSTEMS

Notwithstanding the widespread clinical interest in PET/MR imaging, there are several challenges that face the use of this technology in clinical setting and that may represent inherent limitations in this technique. The primary motivation for multimodality imaging including PET/MRI has been image fusion of molecular and anatomical data to facilitate anatomical localization of functional abnormalities and to assist region-of-interest (ROI) delineation for quantitative analysis.[15,126] However, the anatomical information can also be useful for many other tasks including, attenuation compensation, transmission-based scatter modeling, motion detection, and correction, introducing *a priori* anatomical information into reconstruction of the PET emission data, and partial volume correction.[127] Given its clinical relevance and

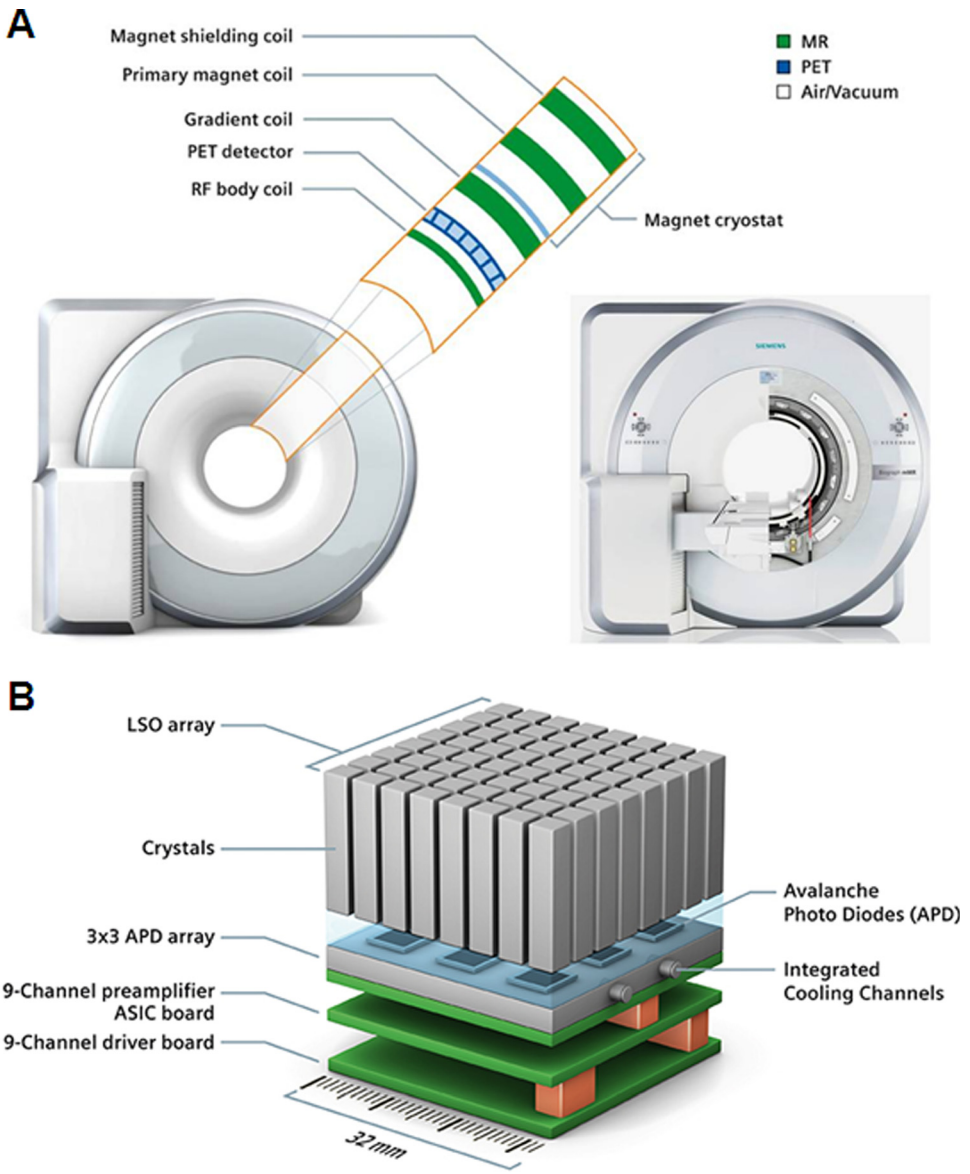

FIG. 9. Artistic view of the whole-body mMR MR-PET prototype (a) showing the basic components of the system where the PET detector ring is placed between the RF coil and the RF body coil. (b). Configuration of the detector block consisting of 8×8 LSO crystals read-out by a matrix of 3×3 APDs. Courtesy of Siemens Healthcare.

the challenges faced, the issue of MR-guided attenuation correction will be discussed in more detail below.

IV.A. MRI-guided attenuation correction

The use of CT-based[128,129] and more recently MRI-guided[130,131] attenuation compensation has received a great deal of attention in the scientific literature. As discussed earlier, the former has many advantages compared to conventional transmission-based scanning which is now considered obsolete following the advent of hybrid systems.[132] However, CT-based attenuation correction still has many drawbacks that need to be addressed through research including polychromaticity of x-ray photons and beam hardening effect, misregistration between CT and PET images resulting, for instance, from respiratory motion, truncation artifacts, the presence of oral and intravenous contrast medium, metallic implants, x-ray scatter in CT images, and other CT artifacts from any source.[133] On the other hand, the limited space available on PET/MRI units makes placement of external radionuclide sources difficult or even impossible. This has spurred the development of MRI-guided attenuation correction, which is still in its infancy and remains challenging for whole-body imaging.[130,131] This is a very active research topic that will certainly impact the future of hybrid PET/MRI technology.

The expanding diagnostic and therapeutic applications of quantitative PET imaging have motivated the development of sophisticated scatter correction techniques, which incorporate patient-specific attenuation maps derived from either CT or MR image and the physics of interaction and detection of emitted photons to estimate the scatter magnitude and distribution accurately.[134] Transmission-based scatter correction methods use an attenuation map to define the inhomogeneous

properties of the scattering object and derive a distribution of scattered events using line integrals calculated as part of the attenuation correction method. Algorithms belonging to this class of model-based methods have been successfully applied in a clinical setting.[135–138] Although computationally intensive, more refined algorithms that use a patient-specific attenuation map, an estimate of the emission image and Monte Carlo-based radiation transport calculations to estimate the magnitude and spatial distribution of Compton scattered events that would be detected were also considered.[139–141]

The major difficulty facing MRI-guided attenuation correction lies in the fact that the MR signal or tissue intensity level is not directly related to electron density, which renders conversion of MR images to attenuation maps less obvious compared to CT. The basic problem of attenuation map determination from MRI is to locate and map the major attenuating structures in the body. Theoretically, this can be achieved in two steps: segmentation into regions of tissues/organs having different attenuating properties and assignment of corresponding linear attenuation coefficients at 511 keV to the segmented tissues/organs. Some of the problematic tissues in whole-body imaging are bone and brain skull, the lungs and other unpredictable benign or malignant anatomical abnormalities with varying densities. Bone is intrinsically not detectable by conventional MR sequences (except dedicated sequences such as ultrashort echo time—UTE) as it provides a black or void "signal," making it difficult to distinguish air from bone. However, in the head, the skull bone is covered by subcutaneous fat and encloses the brain. Incorporation of *a priori* anatomic knowledge allows for sufficient information to be collected to precisely segment MR scans and thus to provide an accurate attenuation map. More sophisticated bone segmentation techniques using active shape models might help to circumvent the limitations discussed above.[142,143] Ignoring bone was reported to be acceptable in the abdomen and hip regions[144–146] but certainly not in the thorax.[147]

Early attempts aimed to construct a nonuniform attenuation map from MRI for brain PET imaging relied on the use of segmented T1-weighted 3-D MR images.[148] The technique was further refined by automating the segmentation of the skull procedure of T1-weighted MRI[149,150] using a sequence of mathematical morphological operations.[151] Another appealing approach for segmentation of the skull and bony structures is to use multispectral MR data acquisition with varying contrast characteristics to provide additional information for distinguishing between different tissues. For example, T1-weighted images show better soft-tissue contrast, whereas T2-weighted images show bony structures more clearly. The development of more refined MR sequences to label the bone structure more precisely (e.g., UTE sequences) will certainly play a significant role in novel methodological developments aiming at deriving attenuation maps from MR images.[152,153] Careful optimization of the MR sequences is a prerequisite for successful implementation of the technique and needs to be investigated further. However, long acquisition times make acquisition of more than one MR sequence (as needed for some segmentation algorithms) unpractical. Segmentation of lung regions in thoracic MR imaging is another challenging issue that has received little attention.[154] With respect to MRI-guided attenuation correction, the lung is one of the most challenging organs given that it has been shown that the density of lung tissue is considerably different from subject to subject, depends on breathing patterns and varies with age and in the event of respiratory diseases by as much as 30%.[155]

Another approach is to use representative anatomical atlas registration where the MRI atlas is registered to the patient's MRI and prior knowledge of the atlas' attenuation properties (for example, through coregistration to CT atlas) is used to yield a patient-specific attenuation map.[156] The critical and crucial part of the algorithm is the registration procedure, which might fail in some cases with large deformations.[157] The second fundamental question that remains to be addressed is: does the global anatomy depicted by an atlas really predict individual attenuation map? The use of support vector machines to predict the attenuation coefficients directly from the local image information by training a machine learning algorithm using small image patches has been reported recently.[158] Combination of this approach with the atlas registration described above might be an appealing technique. Despite the promising results presented so far, more research is still needed to fully automate the procedure and to render it applicable to whole-body imaging.[130] Moreover, the clinical applicability of this approach remains to be demonstrated.

Atlas-based methods rely on registration of the undergoing MR data to a set of MR images in the training dataset that has corresponding CT images to create pseudo-CT image.[158] While atlas-based methods are proclaimed to be more accurate, they suffer from massive computation cost and sensitivity to anatomic variations of structures. Segmentation-based methods are robust but suffer from limited precision in the derivation of attenuation coefficients owing to the limited number of segmented clusters.[131] It is not clear whether the segmentation-based approach outperforms the atlas-guided technique. A comparative study between both approaches is indeed worth to be performed.

The fully automated three-segment (background air, soft tissue, and lung) technique implemented on the Philips Ingenuity TF PET/MRI system[75] seems to be suitable for clinical whole-body imaging.[145] It uses the so-called atMR acquisition protocol (Philips sequence for anatomical mapping and attenuation correction purposes) and consists of a fast multistack whole-body protocol, which takes about 4 min for 100 cm axial coverage. This is a 3D multistack spoiled T1-weighted gradient echo sequence with flip angle 10°, TE 2.3 ms, TR 4.1 ms, smallest water-fat shift, 600 mm transverse FOV with a slab thickness of 120 mm, voxel size $3 \times 3 \times 6$ mm^3, and 12 mm overlap between adjacent stacks. The atMR acquisition on its own is not intended to be of diagnostic quality. The attenuation correction algorithm offers robust extraction of the outer contour of the body and the lungs. Figure 10 shows the above described T1 weighted gradient echo MRI sequence coregistered to CT image of the same patient, the three-segment (soft tissue, lung, and air)

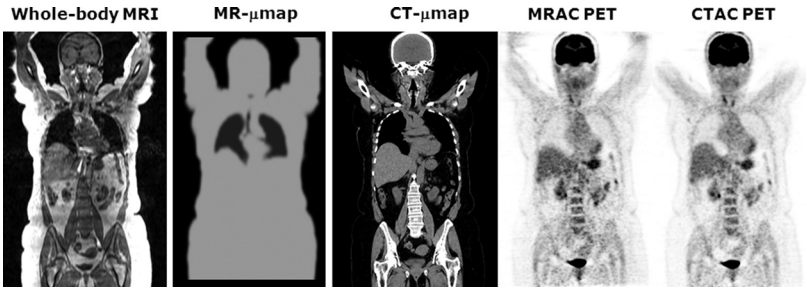

FIG. 10. From left to right, whole-body T1 weighted gradient echo MRI sequence coregistered to CT image of the same patient, derived three-segment (soft tissue, lung, and air) attenuation map (MRAC), CT-based attenuation map (CTAC), and attenuation-corrected PET images using MRAC and CTAC.

attenuation map (MRAC) derived from the image shown on the left, CT-based attenuation map (CTAC) obtained on clinical PET/CT scanner, and attenuation-corrected PET images using MRAC and CTAC, respectively.

Another technique considers a four-class attenuation map (background, lungs, fat, and soft tissue), which requires the acquisition of a two-point Dixon MR sequence.[144] A similar four-class segmentation approach is implemented on the Siemens mMR MR-PET scanner, although the detailed technical specifications of this algorithm are unknown to the authors. The largest SUV changes (<15% on average) were reported in lesions located in the bone.[144–146] The MRAC validation procedure is illustrated in Fig. 11 where the MRAC map obtained on the PET/MRI scanner was modified by removing the scanner table template and then coregistered using a nonrigid deformable algorithm[159] to the CTAC map, then the CT scanner bed was added. The PET data were then reconstructed using both attenuation maps.

Other challenging issues that remain to be explored include contrast instability of MR compared to CT, misclassification issues and inaccuracies associated with assigning theoretical attenuation coefficients and neglecting some biological tissues (e.g., bone), motion artifacts, attenuation of MR hardware (e.g., MR table, RF coils. Pillows, headphones, medical probes, and all the items that are MR invisible but contribute to photon attenuation),[160,161] other patient positioning aids[162] present in the field-of-view, and conductive MR compatible or even nonconductive but MR invisible implants. Truncation in the transverse plane owing to the limited size of the MR field-of-view leads to incomplete attenuation maps, thus causing artifacts in the reconstructed PET image. The proposed techniques rely on the nonattenuation corrected (NAC) PET images as starting point to derive attenuation properties of the body outside the MR FOV by segmenting the body contour using active contour models to fill the truncated parts of the attenuation map.[163] Another technique uses a MAP (or penalized likelihood) approach to estimate the missing truncated part of the attenuation map from the PET emission data, together with the unknown activity distribution.[164] It has been shown that PET images are less sensitive to attenuation artifacts when reconstructed with TOF information.[165] The latter study reported the NAC-TOF images were more uniform than the non-TOF images and that the use of TOF-NAC may be useful in providing more interpretable images in some situations were an attenuation map is impossible to obtain, or introduces noticeable errors. The TOF property is exploited by Salomon *et al.*[166] using an iterative reconstruction approach to simultaneously estimate the activity concentration (via maximum-likelihood estimation) and attenuation distribution (via gradient-ascent based algorithm) using the segmented MR image as anatomical reference. An obvious advantage of this technique is that it obviates the need of incorporating additional anatomical *a priori* information and as such, it is not affected by issues such as person-specific tissue attenuation variability and unpredictable anatomical abnormalities.

IV.B. MRI-guided PET image reconstruction

An undesirable property of the statistical iterative reconstruction techniques including the popular maximum-likelihood—expectation maximization algorithm (ML-EM) is that large numbers of iterations increase the noise content of the reconstructed PET images.[167] The noise characteristics can be controlled by incorporating a prior distribution to describe the statistical properties of the unknown image and thus produce *a posteriori* probability distributions from the image conditioned upon the data. Bayesian reconstruction methods form a powerful extension of the ML-EM algorithm. Maximization of the *a posteriori* (MAP) probability over the set of possible images results in the MAP estimate.[168] This approach has many advantages since the

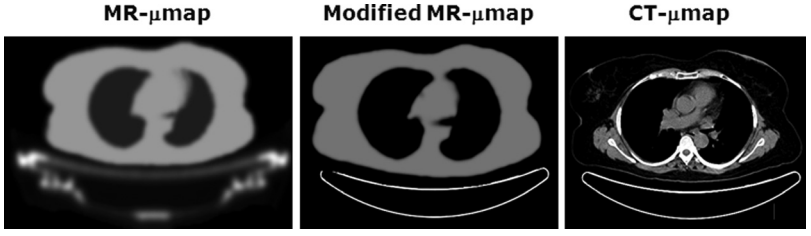

FIG. 11. Attenuation correction maps derived from segmentation of T1-weighted MRI followed by assignment of known linear attenuation coefficients to the lung and soft tissue and addition of the scanner table template (left), same image shown on the left after nonrigid alignment to the CT attenuation map following removal of the PET/MR bed and addition of the CT scanner bed CT (middle), and the CT-based attenuation map (right) of the same patient.

various components of the prior, such as pseudo-Poisson nature of statistics, non-negativity of the solution, local voxel correlations (local smoothness), or known existence of anatomical boundaries, may be added one by one into the estimation process, assessed individually, and used in the practical implementation of the algorithms. A Bayesian model can also incorporate prior anatomical information derived from a registered CT (Ref. 169) or MRI (Refs. 78 and 170) image in the reconstruction of PET data with the aim to avoid resolution loss due to the regularization, yet to recover the resolution exploiting the superior resolution of the anatomical images.

This class of algorithms incorporates a coupling term in the reconstruction procedure that favors the formation of edges in the PET data that are associated with the location of noteworthy anatomical edges from the anatomical images. A Gibbs prior distribution is usually utilized to encourage the piecewise smoothness of reconstructed PET images. A Gibbs prior of piecewise smoothness can also be incorporated in the Bayesian model. Some groups have published preliminary promising results with segmentation-free anatomical priors based on measures similar to mutual information, but further investigation is required. In this way, the development of dual-modality imaging systems producing accurately registered anatomical and functional image data is motivating the further investigation of the potential of Bayesian MAP reconstruction techniques. MRI-guided PET image reconstruction in brain imaging outperforms CT-guided reconstruction owing to the high soft-tissue contrast provided by MR and the accuracy obtained using sophisticated brain MRI segmentation procedures available today.[127] The potential of x-ray CT for this purpose in whole-body PET/CT seems to be limited in this respect with only limited preliminary results presented so far.[169]

More recently, a new MAP reconstruction method for PET image reconstruction was proposed.[171] The algorithm incorporates MR image information with the joint entropy between the PET and MR image features serving as the regularization constraint. A nonparametric method is then used to estimate the joint probability density of the PET and MR images. It has been shown that the incorporation of the anatomic information using this approach, after parameter optimization, results in remarkable improvement of the noise versus bias tradeoff in region-of-interest-based quantitative analysis, compared to the results obtained using conventional MAP reconstruction.

IV.C. MRI-guided partial volume effect correction

The quantitative accuracy of PET is hampered by the low spatial resolution capability of currently available clinical scanners. The well accepted criteria is that one can accurately quantify the activity concentration for sources having dimensions equal or larger than twice the system's spatial resolution measured in terms of its FWHM. Sources of smaller size only partly occupy this characteristic volume and as such, the counts are spread over a larger volume than the physical size of the object owing to the limited spatial resolution of the imaging system. It should be noted that the total number of counts is conserved in the corresponding PET images. In this case, the resulting PET images reflect the total amount of the activity within the object but not the actual activity concentration. This phenomenon is referred to as the partial volume effect (PVE) and can be corrected using one of the various strategies developed for this purpose.[5,172] The simplest technique uses recovery coefficients determined in a calibration measurement for objects of simple geometrical shape.[173] This technique works relatively well for objects that can be approximated by simple geometrical shapes (e.g., tumors of spherical shape).[174] More sophisticated anatomy-based postreconstruction approaches were also developed to correct for this effect knowing the size and shape of the corresponding structures as assessed by structural imaging (MRI or CT).[175,176]

In the context of multimodality brain imaging, a main concern has been related to the PVE correction for cerebral metabolism in the atrophied brain, particularly in Alzheimer disease (AD). Figure 12 illustrates the impact of voxel-based MRI-guided PVE correction in functional FDG-PET brain imaging of a patient with probable AD using the approach by Matsuda *et al.*[177] The procedure involves realigning the

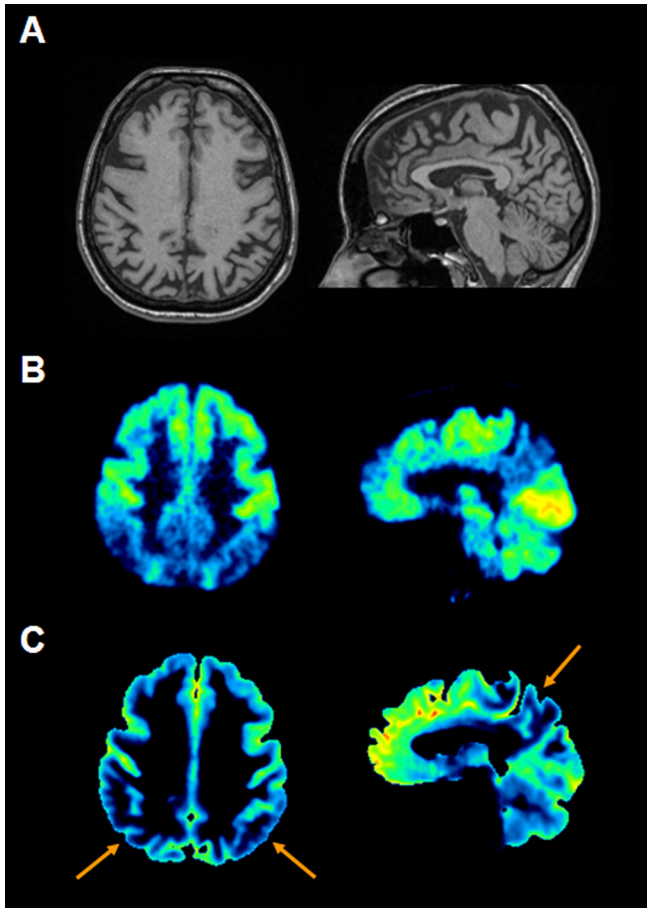

FIG. 12. Illustration of MRI-guided partial volume correction impact in functional brain PET imaging showing for a patient with probable Alzheimer's disease the original T1-weighted MRI (a) and PET image before (b) and after partial volume effect correction (c). The arrows put in evidence that the hypometabolism extends beyond the atrophy.

PET and MR image volumes followed by segmenting the MR image into white and grey matters. The next step of this correction method consists in convolving the segmented white and grey matter images by the PET scanner's spatial resolution modeled by a Gaussian response function. The grey matter PET image is then obtained by subtraction of convolved PET white matter image from the original PET image. The partial volume effect corrected grey matter PET image is then obtained by dividing the grey matter PET image by the convolved grey matter MR image. A binary mask for grey matter is finally applied.

The accuracy of MRI-guided PVE correction in PET largely depends on the accuracy achieved by the PET/MRI coregistration procedure, which will be improved by using simultaneous hybrid PET/MRI systems. The second issue impacting the accuracy of MRI-guided partial volume correction in brain PET is the MR segmentation procedure. In this context, the high soft-tissue contrast of MR allows the differentiation between grey and white matter. The impact of brain MR image segmentation on partial volume correction was investigated by Zaidi *et al.*[127] Inaccuracies resulting from mis-segmentation can be considered in the context of a more general problem of tissue heterogeneity. In fact, the key limiting factor of these techniques is mainly the hypothesis made regarding the homogeneity of tracer distribution in each region or tissue component.

More recent techniques using multiresolution synergetic approaches that combine functional and anatomical information from various sources appear promising and should be investigated further in a clinical setting.[178] The corrections for the PVE can also be applied during the reconstruction process by incorporating a mathematical model for PVE along with other physical perturbations (photon attenuation, scattered radiation, and other physical effects) directly into the reconstruction algorithm.[179]

IV.D. MRI-guided motion correction

With the spatial resolution achieved on modern high resolution PET scanners available today, the development and implementation of accurate patient motion correction strategies became essential in clinical setting. Advanced motion correction methods for the three cases of (1) unwanted patient motion, as well as motions due to (2) cardiac, and (3) respiratory cycles are described elsewhere.[180] Broadly, three types of general approaches were reported in the literature: (1) nonrigid registration of independently reconstructed images, (2) initial estimation of the motion information from the gated PET or MR/CT images, which is subsequently used in a new reconstruction applied to all the gated frames, and (3) simultaneous estimation of the motion parameters and the images.

Patient motion (either voluntarily or involuntarily) between or during the anatomical and functional image acquisitions remains a major challenge for PET/MR imaging protocols. The typical misalignment between PET and CT images at the level of the diaphragm on combined PET/CT scanners owing to differences between breathing protocols will likely be partly addressed through the introduction of PET/MRI owing to the longer acquisition time of typical MR sequences used for attenuation correction, thus leading to temporal averaging that would, not necessarily, but in some cases improve the alignment between MRI and PET. The PET/MRI can improve the matching of PET and MR data by the use of a defined respiratory protocol. A PET image alone corresponds to an average of multiple respiratory cycles and is susceptible to motion-related distortion. Likewise, typical MR data which are used for attenuation correction produce an image from an average of fewer respiratory cycles but carrying a lot of motion compared to CT. It should be emphasized that the averaging process in MRI is not comparable to the process involved with PET. Even more, if the motion is too high, motion artifacts appear and consequently organs which are subject to motion will appear smaller on the MR derived attenuation map compared to CT. Moreover, the result is an image carrying more visual noise and not very useful for clinical diagnosis. The requirement for effective attenuation correction, as well as improved spatial resolution, is that PET and MR data correspond to the same respiratory phase and spatial details, without which the MR-based attenuation-corrected PET images would be inaccurate. Therefore, an incongruent lesion position during MR acquisition will induce misregistration and incorrect anatomical localization and more importantly bias activity estimates using PET. In order to correlate PET and MR at a certain respiratory phase, the patient's breathing throughout MR scanning needs to be regulated to minimize the distortional effects of respiratory movement. The breathing protocol involves coaching patients on their breathing before they are scanned.

Various MRI motion tracking techniques particularly for rigid-body motion are being used in clinical setting including but not limited to embedded cloverleaf navigators.[181] Such techniques have been used on the brain PET/MRI prototype where high-temporal-resolution MRI-derived motion estimates obtained, while simultaneously acquiring anatomic or functional MRI data are used for motion correction of corresponding brain PET data.[76] Recent efforts focus on 4D MR-derived motion correction schemes to eliminate artifacts seen in PET/CT by developing MR-based motion-compensated PET attenuation correction strategies. Careful work must be done to design protocols to reduce MR artifacts, while minimizing the mismatch between the MR and PET data. The scheme consists in correcting PET images blurred by patient motion through motion estimated from MR images to obtain motion free PET images. Acquired MR data can then be used to correct for motion in PET. It has been demonstrated that motion artifacts will be significantly reduced thus enabling more accurate PET image quantification and improvement in image quality through the use of MR motion fields, compared to the use of PET-only motion information.[182] Novel 3D cine MR sequences have been developed by several groups to track the position and deformation of organs (e.g., the heart or thorax), which can be used to generate deformation fields for direct incorporation in statistical iterative PET reconstruction algorithms.[183,184] It

should be emphasized that the difficulty of obtaining dynamic MR images of a large enough ROI with sufficient spatial and temporal resolution for motion correction has led to the investigation of possible surrogates.

Tsoumpas *et al.*[182] reported significant reduction of motion artifacts and substantial improvement of PET image quality and quantitative accuracy through the use of MR motion fields compared to the use of motion information derived only from PET. They concluded that combined PET/MRI acquisitions potentially allow nonrigid motion compensation in whole-body PET acquisitions without increasing acquisition time. Using 3D Hoffman brain phantom and human volunteer studies, Catana *et al.*[76] reported that high-temporal-resolution MRI-derived motion estimates acquired simultaneously on the hybrid brainPET scanner can be used to improve PET image quality, thus increasing its reliability, reproducibility, and quantitative accuracy.

V. CLINICAL RELEVANCE OF PET/MRI

The clinical role of multimodality imaging encompasses a wide variety of applications and now is performed routinely with commercially available radiopharmaceuticals to answer important clinical questions including those in oncology,[2,185] cardiology,[186,187] neurology, and psychiatry.[188,189] Nowadays, a plethora of novel tracers are used routinely for assessing tumor metabolism and other biological and physiological parameters associated with many diseases[1,190] that have clearly demonstrated the enormous potential of emerging hybrid technologies in the field of molecular imaging.

As discussed earlier, much of multimodality imaging with special emphasis on PET/MRI fusion was restricted to intrasubject brain applications, where the confinement of compact brain tissues within the skull renders a rigid-body model a satisfactory approximation.[191,192] Therefore, correlative PET/MR imaging techniques were introduced in the clinic, mostly for neuroimaging applications, well before the advent of hardware-based PET/MR imaging. Multimodality imaging played a pivotal role in the assessment of central nervous system disorders such as seizures, Alzheimer and Parkinson diseases, head injury, and inoperable brain tumors.[193–195]

Correlated FDG-PET and anatomical T1/T2-weighted MRI studies are generally used for the evaluation of epilepsy to allow accurate localization of the epileptogenic focus. Similar approaches are used in the evaluation of neurodegenerative diseases including dementia. Likewise, in the neuro-oncology field, dedicated tracers including amino acids (e.g., ^{18}F-fluoro-ethyl-tyrosine) are used in conjunction with anatomical MRI for biological tumor volume delineation for the purpose of radiation therapy treatment planning.[196] This kind of PET/MR image registration and fusion techniques has been a standard component of many clinical practices for the last two decades and is used routinely in many institutions. However, corresponding techniques for other regions of the body have not achieved the same widespread clinical use.

The limited role of PET/CT in some clinical indications including central nervous system disorders, orthopedic infections, and inflammatory disorders and in the evaluation and follow-up of metastatic disease is well established. In this respect, the potential of the simultaneous hybrid brain PET/MRI system[49] was explored for a relatively limited applications including brain tumors[197] using ^{11}C-methionine[198] and ^{68}Ga-DOTATOC (Ref. 199) and more recently head and neck tumors.[200] Moreover, it has recently been demonstrated that high resolution combined PET/MRI allow substructure-specific metabolic activities in the thalamus to be measured accurately.[201] Figure 13 shows representative clinical brain PET/CT and PET/MR images of a normal subject acquired sequentially on two combined systems, namely Biograph TrueV (Siemens Healthcare) and Ingenuity TF PET/MRI (Philips Healthcare). The PET/CT study started 30 min following injection of 370 MBq of ^{18}F-FDG followed by PET/MRI, which started about 80 min later. The better soft-tissue contrast observed on MRI is obvious and further emphasizes

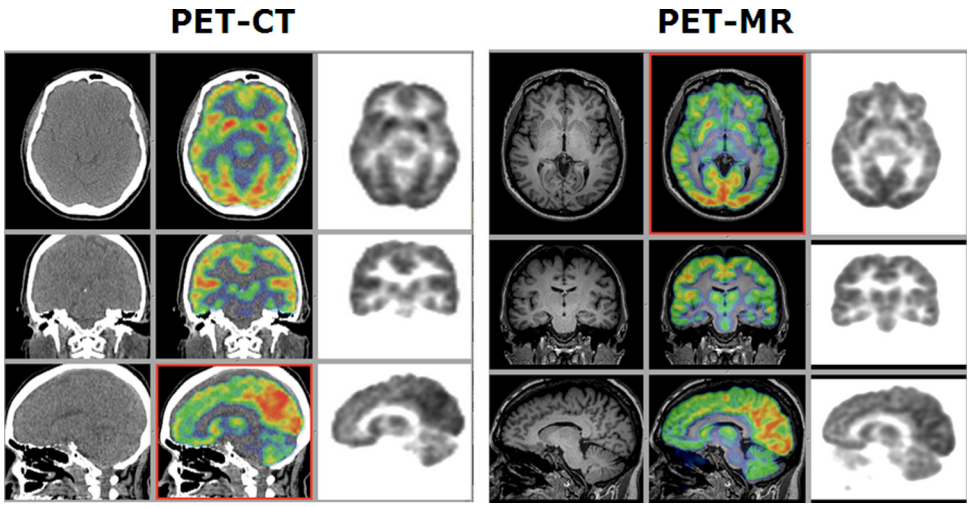

FIG. 13. Representative clinical PET/CT (left) and PET/MR (right) brain images of a normal subject acquired sequentially (~80 min time difference) on two combined systems (Siemens Biograph TrueV and Philips Ingenuity TF PET/MRI, respectively) following injection of 370 MBq of ^{18}F-FDG. Courtesy of Geneva University Hospital.

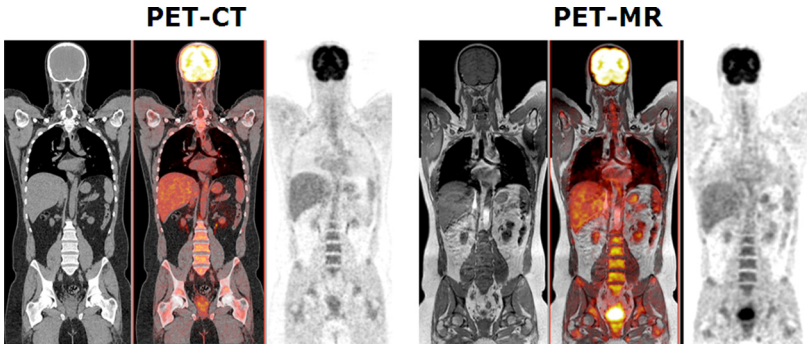

FIG. 14. Representative clinical PET/CT (left) and PET/MR (right) whole-body images of the same patient acquired sequentially (~60 min time difference) on two combined systems (Siemens Biograph Hirez TrueV and Philips Ingenuity TF PET/MRI, respectively) following injection of 370 MBq of ^{18}F-FDG. Courtesy of Geneva University Hospital.

the ineffectiveness of PET/CT for this indication and the potential role of PET/MRI.

Despite the fact that the clinical role of PET/MRI in clinical setting is controversial and has not been yet addressed properly, the prospective applications of a whole-body PET/MRI system in clinical oncology have been explored in the literature.[54–72] The potential of nanoparticle-based dual-modality PET/MRI contrast agents is also being investigated.[202] Figure 14 shows a representative whole-body PET/CT and PET/MRI studies of the same patient acquired sequentially where the PET/CT started approximately 60 min following injection of 370 MBq of ^{18}F-FDG. The time delay between the PET/CT and PET/MRI studies was ~60 min. Both studies presented with comparable image quality leading to similar findings. The lesions detected at PET/CT were also identified by PET/MRI, with small difference between PET/CT and PET/MRI uptake ratios.

Some scientific arguments on the advantages of simultaneous imaging of morphological and functional information using hybrid PET/MRI technology will improve tissue characterization. However, many challenging issues still need to be addressed including the clinical relevance and justification for this technology. We learned from the history of multimodality imaging that any new technology should be assessed carefully with respect to benefits conveyed to patients before widespread acceptance and adoption. Large-scale studies are needed to demonstrate the clinical benefits of PET/MRI and, to define where more widespread PET/CT systems are sufficient and where PET/MRI is needed.

In addition to offering a diversity of tissue contrasts, MRI will provide a wealth of additional information through fMRI and MRS to enhance the diagnostic performance and quantitative capabilities of PET. More importantly, using simultaneous (rather than sequential) scanning will enable to resolve many of the impediments to precise coregistration of anatomomolecular information and accurate attenuation correction. Second, reimbursement issues were mainly driven by prospective clinical studies that demonstrate improvements in health outcomes conveyed by an imaging modality for a given indication. Therefore, given the higher soft-tissue contrast resolution of MRI and its highest sensitivity and specificity for many indications, coverage for PET scans will undoubtedly be expanded.

The strategies for clinical validation of novel multimodality imaging technologies including PET/MRI are not well established and are often dictated by regulations imposed by regulatory bodies. Usually the Food and Drug Administration (FDA) in the U.S. requires a certain number of patients scanned using a well defined protocol to demonstrate the safety and clinical relevance of novel technologies through comparison with a well established imaging modality used as reference for comparison. The Ingenuity TF PET-MRI system (Philips Healthcare) already obtained the CE mark (European regulator) early this year, whereas the mMR system (Siemens Healthcare) obtained the CE mark and FDA approval in June 2011.

VI. CONCLUDING REMARKS AND FUTURE PROSPECTS

There is no doubt that multimodality imaging had changed drastically over the last two decades. The pace of change has accelerated rapidly in the last decade driven by the introduction and widespread acceptance of combined PET/CT units in the clinic and the likely deployment of compact PET/MRI systems in the near future. The recent introduction of hybrid PET/MRI technology is considered by many experts as a major breakthrough that will potentially lead to a revolutionary paradigm shift in healthcare and revolutionize clinical practice.[11,15] Several active research groups in academic and corporate settings are focusing on the development of various configurations of MR-compatible PET inserts to allow simultaneous scanning using the most highly sophisticated molecular imaging technologies available today. The requests imposed to the instrumentation by a simultaneous PET/MRI scanner have triggered the use of innovative and promising technologies that will outperform currently existing detectors. The PET detector module should have a flexibility to allow its use in both preclinical and clinical applications. The high granularity of the photodetector, adapted to each application, will result in an improvement of the spatial resolution. The fast response of the scintillators and the photodetectors employed, and a dedicated ASIC that preserves these properties, will result in a fast detector module, making possible implementation of the TOF technique in clinical PET, with a significant reduction of image noise and consequent improvement of image quality. In the case of preclinical imaging, given the small size of the organs of rodents (mice and rats), a high spatial resolution is of utmost importance. An MR compatible detector module needs to have a high intrinsic spatial resolution and DOI capability for parallax error reduction that will result in a truly submillimeter PET spatial

resolution. A high sensitivity would also be desired since this is the factor limiting the effective spatial resolution at the small voxel volumes. The implementation of a new block detector in a fully simultaneous PET/MRI scanner will certainly open new possibilities in preclinical and clinical studies, research, diagnosis, therapy, and follow-up.

Finally, the advances in PET/MRI have also triggered research in SPECT/MR hybrid scanners, where direct photon conversion detectors such as CdZnTe are mostly used. The first prototypes for small-animal imaging are now available.[203–205] SPECT/MR will provide an additional and improved multimodality information to the hybrid imaging field in the near future.

The future of hybrid PET/MR imaging lies in the development of systems that make multimodality and multiparametric imaging simple, easy, and reproducible. The target information is not so much pretty images, but rather the information content related to how much probe went to what specific location. PET/MR imaging systems will expand to incorporate MR-compatible devices required for various purposes and to consider these devices during the MRI-guided attenuation correction procedure.

The production of fused coregistered images from multiple modalities including PET and MRI will become increasingly automated and requires less user interaction. The images themselves will become increasingly less emphasized as the content becomes the focus, shifting from images to relevant data about timing and uptake information (parametric). The future will likely see a shift toward the end user offering the possibility to operate these systems by minimally trained personnel with little or no support required to analyze the imaging-based data. One issue does remain clear, which is that the more information that can be obtained, whether sequentially or simultaneously, the better a biological system can be understood. Often the imaging modalities are complementary, providing different information about the disease, thus multimodality is likely to become the normal way imaging-based clinical diagnosis and research is conducted in the future.

Thus, many different design paths have been and continue to be pursued in both academic and corporate settings, that offer different trade-offs in terms of their performance. It still is uncertain, which designs will be incorporated into future clinical and research systems, but it is certain that technological advances will continue and will enable novel applications of multimodality and multiparametric imaging.

ACKNOWLEDGMENTS

This work was supported by the Swiss National Science Foundation under Grant Nos. SNSF 31003A-125246 and 33CM30-124114, and Geneva Cancer League (HZ) and by the Italian National Institute of Nuclear Physics-DaSiPM2 project and European Community in the framework of the FP7 ENVISION project (ADG).

[a]Author to whom correspondence should be addressed. Electronic mail: habib.zaidi@hcuge.ch; Telephone: +41 22 372 7258; Fax: +41 22 372 7169.

[1]J. F. Valliant, "A bridge not too far: Linking disciplines through molecular imaging probes," J. Nucl. Med. **51**(8), 1258–1268 (2010).
[2]R. Weissleder and M. J. Pittet, "Imaging in the era of molecular oncology," Nature (London) **452**(7187), 580–589 (2008).
[3]T. Jones, "Molecular imaging with PET—The future challenges," Br. J. Radiol. **75**(90009), S6–S15 (2002).
[4]C. C. Meltzer, P. E. Kinahan, P. J. Greer, T. E. Nichols, C. Comtat, M. N. Cantwell, M. P. Lin, and J. C. Price, "Comparative evaluation of MR-based partial-volume correction schemes for PET," J. Nucl. Med. **40**(12), 2053–2065 (1999).
[5]O. Rousset, A. Rahmim, A. Alavi, and H. Zaidi, "Partial volume correction strategies in PET," PET Clin. **2**(2), 235–249 (2007).
[6]D. L. Hill, P. G. Batchelor, M. Holden, and D. J. Hawkes, "Medical image registration," Phys. Med. Biol. **46**(3), R1–R45 (2001).
[7]T. Beyer, D. Townsend, T. Brun, P. Kinahan, M. Charron, R. Roddy, J. Jerin, J. Young, L. Byars, and R. Nutt, "A combined PET/CT scanner for clinical oncology," J. Nucl. Med. **41**(8), 1369–1290 (2000).
[8]A. L. Goertzen, A. K. Meadors, R. W. Silverman, and S. R. Cherry, "Simultaneous molecular and anatomical imaging of the mouse in vivo," Phys. Med. Biol. **21**, 4315–4328 (2002).
[9]H. Zaidi, O. Mawlawi, and C. G. Orton, "Point/counterpoint. Simultaneous PET/MR will replace PET/CT as the molecular multimodality imaging platform of choice," Med. Phys. **34**(5), 1525–1528 (2007).
[10]D. W. Townsend, "Multimodality imaging of structure and function," Phys. Med. Biol. **53**(4), R1–R39 (2008).
[11]B. J. Pichler, A. Kolb, T. Nagele, and H. P. Schlemmer, "PET/MRI: Paving the way for the next generation of clinical multimodality imaging applications," J. Nucl. Med. **51**(3), 333–336 (2010).
[12]J. M. Park and S. S. Gambhir, "Multimodality radionuclide, fluorescence, and bioluminescence small-animal imaging," Proc. IEEE **93**(4), 771–783 (2005).
[13]B. Hasegawa and H. Zaidi, "Dual-modality imaging: More than the sum of its components," *Quantitative Analysis in Nuclear Medicine Imaging*, edited by H. Zaidi (Springer, New York, 2006), pp. 35–81.
[14]D. Renker, "Geiger-mode avalanche photodiodes, history, properties and problems," Nucl. Instrum. Methods Phys. Res. A **567**(1), 48–56 (2006).
[15]H. Zaidi, M. L. Montandon, and A. Alavi, "The clinical role of fusion imaging using PET, CT, and MR imaging," Magn. Reson. Imaging Clin. N. Am. **18**(1), 133–149 (2010).
[16]H. Iida, I. Kanno, S. Miura, M. Murakami, K. Takahashi, and K. Uemura, "A simulation study of a method to reduce positron annihilation spread distribution using a strong magnetic field in positron emission tomography," IEEE Trans. Nucl. Sci. **33**, 597–600 (1986).
[17]D. Rickey, R. Gordon, and W. Huda, "On lifting the inherent limitations of positron emission tomography by using magnetic fields (MagPET)," Automedica **14**, 355–369 (1992).
[18]B. E. Hammer, N. L. Christensen, and B. G. Heil, "Use of a magnetic field to increase the spatial resolution of positron emission tomography," Med. Phys. **21**(12), 1917–1920 (1994).
[19]R. R. Raylman, B. E. Hammer, and N. L. Christensen, "Combined MRI-PET scanner: A Monte Carlo evaluation of the improvements in PET resolution due to the effects of a static homogeneous magnetic field," IEEE Trans. Nucl. Sci. **43**(4), 2406–2412 (1996).
[20]A. Blanco, N. Carolino, C. M. B. A. Correia, L. Fazendeiro, N. C. Ferreira, M. F. Ferreira Marques, R. Ferreira Marques, P. Fonte, C. Gil, and M. P. Macedo, "Spatial resolution on a small animal RPC-PET prototype operating under magnetic field," Nucl. Phys. B, Proc. Suppl. **158**, 157–160 (2006).
[21]A. Wirrwar, H. Vosberg, H. Herzog, H. Halling, S. Weber, and H.-W. Muller-Gartner, "4.5 Tesla magnetic field reduces range of high-energy positrons-potential implications for positron emission tomography," IEEE Trans. Nucl. Sci. **44**(2), 184–189 (1997).
[22]D. Burdette, E. Chesi, N. H. Clinthorne, K. Honscheid, S. S. Huh, H. Kagan, C. Lacasta, G. Llosa, M. Mikuz, S. J. Park, W. L. Rogers, A. Studen, and P. Weilhammer, "First results from a test bench for very high resolution small animal PET using solid-state detectors," *IEEE Nuclear Science Symposium Conference Record*, pp. 2376–2380 (2005).
[23]N. L. Christensen, B. E. Hammer, B. G. Heil, and K. Fetterly, "Positron emission tomography within a magnetic field using photomultiplier tubes and light-guides," Phys. Med. Biol. **40**(4), 691–697 (1995).
[24]Y. Shao, S. R. Cherry, K. Farahani, and K. Meadors, "Simultaneous PET and MR imaging," Phys. Med. Biol **42**, 1965–1970 (1997).

[25]R. Slates, K. Farahani, Y. Shao, P. K. Marsden, J. Taylor, P. E. Summers, S. Williams, J. Beech, and S. R. Cherry, "A study of artefacts in simultaneous PET and MR imaging using a prototype MR compatible PET scanner," Phys. Med. Biol. **44**, 2015–2027 (1999).
[26]K. Farahani, R. Slates, Y. Shao, R. Silverman, and S. Cherry, "Contemporaneous positron emission tomography and MR imaging at 1.5 T," J. Magn. Reson. Imaging **9**(3), 497–500 (1999).
[27]S. Yamamoto, S. Takamatsu, H. Murayama, and K. Minato, "A block detector for a multislice, depth-of-interaction MR-compatible PET," IEEE Trans. Nucl. Sci. **52**(1), 33–37 (2005).
[28]J. E. Mackewn, D. Strul, W. A. Hallett, P. Halsted, R. A. Page, S. F. Keevil, S. C. R. Williams, S. R. Cherry, and P. K. Marsden, "Design and development of an MR-compatible PET scanner for imaging small animals," IEEE Trans. Nucl. Sci. **52**(5), 1376–1380 (2005).
[29]R. R. Raylman, S. Majewski, S. S. Velan, S. Lemieux, B. Kross, V. Popov, M. F. Smith, and A. G. Weisenberger, "Simultaneous acquisition of magnetic resonance spectroscopy (MRS) data and positron emission tomography (PET) images with a prototype MR-compatible, small animal PET imager," J. Magn. Reson. **186**(2), 305–310 (2007).
[30]R. R. Raylman, S. Majewski, S. K. Lemieux, S. S. Velan, B. Kross, V. Popov, M. F. Smith, A. G. Weisenberger, C. Zorn, and G. D. Marano, "Simultaneous MRI and PET imaging of a rat brain," Phys. Med. Biol. **51**(24), 6371–6379 (2006).
[31]S. Yamamoto, M. Imaizumi, Y. Kanai, M. Tatsumi, M. Aoki, E. Sugiyama, M. Kawakami, E. Shimosegawa, and J. Hatazawa, "Design and performance from an integrated PET/MRI system for small animals," Ann. Nucl. Med. **24**, 89–98 (2010).
[32]A. J. Lucas, R. C. Hawkes, R. E. Ansorge, G. B. Williams, R. E. Nutt, J. C. Clark, T. D. Fryer, and T. A. Carpenter, "Development of a combined microPET-MR system," Technol. Cancer Res. Treat. **5**(4), 337–341 (2006).
[33]W. B. Handler, K. M. Gilbert, H. Peng, and B. A. Chronik, "Simulation of scattering and attenuation of 511 keV photons in a combined PET/field-cycled MRI system," Phys. Med. Biol. **51**(10), 2479–2491 (2006).
[34]R. C. Hawkes, T. D. Fryer, S. Siegel, R. E. Ansorge, and T. A. Carpenter, "Preliminary evaluation of a combined microPET-MR system," Technol. Cancer Res. Treat. **9**(1), 53–60 (2010).
[35]K. M. Gilbert, T. J. Scholl, W. B. Handler, J. K. Alford, and B. A. Chronik, "Evaluation of a positron emission tomography (PET)-compatible field-cycled MRI (FCMRI) scanner," Magn. Reson. Med. **62**(4), 1017–1025 (2009).
[36]M. Bergeron, J. Cadorette, J. F. Beaudoin, M. D. Lepage, G. Robert, V. Selivanov, M. A. Tetrault, N. Viscogliosi, J. P. Norenberg, R. Fontaine, and R. Lecomte, "Performance evaluation of the LabPET APD-based digital PET scanner," IEEE Trans. Nucl. Sci. **56**(1), 10–16 (2009).
[37]C. Catana, Y. Wu, M. S. Judenhofer, J. Qi, B. J. Pichler, and S. R. Cherry, "Simultaneous acquisition of multislice PET and MR images: Initial results with a MR-compatible PET scanner," J. Nucl. Med. **47**(12), 1968–1976 (2006).
[38]B. J. Pichler, M. S. Judenhofer, C. Catana, J. H. Walton, M. Kneilling, R. E. Nutt, S. B. Siegel, C. D. Claussen, and S. R. Cherry, "Performance test of an LSO-APD detector in a 7-T MRI scanner for simultaneous PET/MRI," J. Nucl. Med. **47**(4), 639–647 (2006).
[39]M. S. Judenhofer, C. Catana, B. K. Swann, S. B. Siegel, W.-I. Jung, R. E. Nutt, S. R. Cherry, C. D. Claussen, and B. J. Pichler, "Simultaneous PET/MR images, acquired with a compact MRI compatible PET detector in a 7 Tesla magnet," Radiology **244**(3), 807–814 (2007).
[40]C. Woody, D. Schlyer, P. Vaska, D. Tomasi, S. Solis-Najera, W. Rooney, J.-F. Pratte, S. Junnarkar, S. Stoll, Z. Master, M. Purschke, S.-J. Park, S. Southekal, A. Kriplani, S. Krishnamoorthy, S. Maramraju, P. O'Connor, and V. Radeka, "Preliminary studies of a simultaneous PET/MRI scanner based on the RatCAP small animal tomograph," Nucl. Instrum. Methods Phys. Res. A **571**(1-2), 102–105 (2007).
[41]M. S. Judenhofer, H. F. Wehrl, D. F. Newport, C. Catana, S. B. Siegel, M. Becker, A. Thielscher, M. Kneilling, M. P. Lichy, M. Eichner, K. Klingel, G. Reischl, S. Widmaier, M. Rocken, R. E. Nutt, H. J. Machulla, K. Uludag, S. R. Cherry, C. D. Claussen, and B. J. Pichler, "Simultaneous PET-MRI: A new approach for functional and morphological imaging," Nat. Med. **14**(4), 459–465 (2008).
[42]B. Ravindranath, S. S. Junnarkar, M. L. Purschke, S. H. Maramraju, X. Hong, D. Tomasi, D. Bennett, K. Cheng, S. S. Southekal, S. P. Stoll, J. F. Pratte, P. Vaska, C. L. Woody, and D. J. Schlyer, "Results from prototype II of the BNL simultaneous PET-MRI dedicated breast scanner," *IEEE Nuclear Science Symposium Conference Record*, pp. 3315–3317 (2009).
[43]T. Frach, G. Prescher, C. Degenhardt, R. de Gruyter, A. Schmitz, and R. Ballizany, "The digital silicon photomultiplier—Principle of operation and intrinsic detector performance," *IEEE Nuclear Science Symposium Conference Record (NSS/MIC)*, pp. 1959–1965 (2009).
[44]C. Degenhardt, G. Prescher, T. Frach, A. Thon, R. de Gruyter, A. Schmitz, and R. Ballizany, "The digital silicon photomultiplier—A novel sensor for the detection of scintillation light," *IEEE Nuclear Science Symposium Conference Record (NSS/MIC)*, pp. 2383–2386 (2009).
[45]B. Dolgoshein, V. Balagura, P. Buzhan, M. Danilov, L. Filatov, E. Garutti, M. Groll, A. Ilyin, V. Kantserov, V. Kaplin, A. Karakash, F. Kayumov, S. Klemin, V. Korbel, H. Meyer, R. Mizuk, V. Morgunov, E. Novikov, P. Pakhlov, E. Popova, V. Rusinov, F. Sefkow, E. Tarkovsky, and I. Tikhomirov, "Status report on silicon photomultiplier development and its applications," Nucl. Instrum. Methods Phys. Res. A **563**(2), 368–376 (2006).
[46]D. P. McElroy, V. Saveliev, A. Reznik, and J. A. Rowlands, "Evaluation of silicon photomultipliers: A promising new detector for MR compatible PET," Nucl. Instrum. Methods Phys. Res. A **571**(1-2), 106–109 (2007).
[47]S. Moehrs, A. Del Guerra, D. J. Herbert, and M. A. Mandelkern, "A detector head design for small-animal PET with silicon photomultipliers (SiPM)," Phys. Med. Biol. **51**(5), 1113–1127 (2006).
[48]D. Renker and E. Lorenz, "Advances in solid state photon detectors," J Instrum. **4**(04), P04004 (2009).
[49]H. P. Schlemmer, B. J. Pichler, M. Schmand, Z. Burbar, C. Michel, R. Ladebeck, K. Jattke, D. Townsend, C. Nahmias, P. K. Jacob, W. D. Heiss, and C. D. Claussen, "Simultaneous MR/PET imaging of the human brain: Feasibility study," Radiology **248**(3), 1028–1035 (2008).
[50]H. Herzog, U. Pietrzyk, N. J. Shah, and K. Ziemons, "The current state, challenges and perspectives of MR-PET," Neuroimage **49**(3), 2072–2082 (2010).
[51]S. J. Holdsworth and R. Bammer, "Magnetic resonance imaging techniques: fMRI, DWI, and PWI," Semin. Neurol. **28**(4), 395–406 (2008).
[52]A. Boss, A. Kolb, M. Hofmann, S. Bisdas, T. Nagele, U. Ernemann, L. Stegger, C. Rossi, H. P. Schlemmer, C. Pfannenberg, M. Reimold, C. D. Claussen, B. J. Pichler, and U. Klose, "Diffusion tensor imaging in a human PET/MR hybrid system," Invest. Radiol. **45**(5), 270–274 (2010).
[53]Z. H. Cho, Y. D. Son, H. K. Kim, K. N. Kim, S. H. Oh, J. Y. Han, I. K. Hong, and Y. B. Kim, "A fusion PET-MRI system with a high-resolution research tomograph-PET and ultra-high field 7.0 T-MRI for the molecular-genetic imaging of the brain," Proteomics **8**(6), 1302–1323 (2008).
[54]H. P. Schlemmer, B. J. Pichler, R. Krieg, and W. D. Heiss, "An integrated MR/PET system: Prospective applications," Abdom. Imaging **34**(6), 668–674 (2009).
[55]S. Punwani, S. A. Taylor, A. Bainbridge, V. Prakash, S. Bandula, E. De Vita, O. E. Olsen, S. F. Hain, N. Stevens, S. Daw, A. Shankar, J. B. Bomanji, and P. D. Humphries, "Pediatric and adolescent lymphoma: Comparison of whole-body STIR half-Fourier RARE MR imaging with an enhanced PET/CT reference for initial staging," Radiology **255**(1), 182–190 (2010).
[56]V. Laurent, G. Trausch, O. Bruot, P. Olivier, J. Felblinger, and D. Regent, "Comparative study of two whole-body imaging techniques in the case of melanoma metastases: Advantages of multi-contrast MRI examination including a diffusion-weighted sequence in comparison with PET-CT," Eur. J. Radiol. **75**(3), 376–383 (2010).
[57]T. A. Heusner, S. Kuemmel, A. Koeninger, M. E. Hamami, S. Hahn, A. Quinsten, A. Bockisch, M. Forsting, T. Lauenstein, G. Antoch, and A. Stahl, "Diagnostic value of diffusion-weighted magnetic resonance imaging (DWI) compared to FDG PET/CT for whole-body breast cancer staging," Eur. J. Nucl. Med. Mol. Imaging **37**(6), 1077–1086 (2010).
[58]W. Chen, W. Jian, H. T. Li, C. Li, Y. K. Zhang, B. Xie, D. Q. Zhou, Y. M. Dai, Y. Lin, M. Lu, X. Q. Huang, C. X. Xu, and L. Chen, "Whole-body diffusion-weighted imaging vs. FDG-PET for the detection of non-small-cell lung cancer. How do they measure up?," Magn. Reson. Imaging **28**(5), 613–620 (2010).
[59]D. Takenaka, Y. Ohno, K. Matsumoto, N. Aoyama, Y. Onishi, H. Koyama, M. Nogami, T. Yoshikawa, S. Matsumoto, and K. Sugimura, "Detection of bone metastases in non-small cell lung cancer patients: Comparison of whole-body diffusion-weighted imaging (DWI), whole-body MR imaging without and with DWI, whole-body FDG-PET/CT, and bone scintigraphy," J. Magn. Reson. Imaging **30**(2), 298–308 (2009).
[60]A. Stecco, G. Romano, M. Negru, D. Volpe, A. Saponaro, S. Costantino, G. Sacchetti, E. Inglese, O. Alabiso, and A. Carriero, "Whole-body

diffusion-weighted magnetic resonance imaging in the staging of oncological patients: Comparison with positron emission tomography computed tomography (PET-CT) in a pilot study," Radiol. Med. **114**(1), 1–17 (2009).
[61]G. P. Schmidt, A. Baur-Melnyk, A. Haug, S. Utzschneider, C. R. Becker, R. Tiling, M. F. Reiser, and K. A. Hermann, "Whole-body MRI at 1.5 T and 3 T compared with FDG-PET-CT for the detection of tumour recurrence in patients with colorectal cancer," Eur. Radiol. **19**(6), 1366–1378 (2009).
[62]G. Antoch and A. Bockisch, "Combined PET/MRI: A new dimension in whole-body oncology imaging?," Eur. J. Nucl. Med. Mol. Imaging **36**(Suppl 1), 113–120 (2009).
[63]C. A. Yi, K. M. Shin, K. S. Lee, B.-T. Kim, H. Kim, O. J. Kwon, J. Y. Choi, and M. J. Chung, "Non-small cell lung cancer staging: Efficacy comparison of integrated PET/CT versus 3.0-T whole-body MR imaging," Radiology **248**(2), 632–642 (2008).
[64]G. P. Schmidt, A. Baur-Melnyk, A. Haug, V. Heinemann, I. Bauerfeind, M. F. Reiser, and S. O. Schoenberg, "Comprehensive imaging of tumor recurrence in breast cancer patients using whole-body MRI at 1.5 and 3 T compared to FDG-PET-CT," Eur. J. Radiol. **65**(1), 47–58 (2008).
[65]Y. Ohno, H. Koyama, Y. Onishi, D. Takenaka, M. Nogami, T. Yoshikawa, S. Matsumoto, Y. Kotani, and K. Sugimura, "Non-small cell lung cancer: Whole-body MR examination for M-stage assessment—Utility for whole-body diffusion-weighted imaging compared with integrated FDG PET/CT," Radiology **248**(2), 643–654 (2008).
[66]G. P. Schmidt, H. Kramer, M. F. Reiser, and C. Glaser, "Whole-body magnetic resonance imaging and positron emission tomography-computed tomography in oncology," Top Magn. Reson Imaging **18**(3), 193–202 (2007).
[67]C. Pfannenberg, P. Aschoff, S. Schanz, S. M. Eschmann, C. Plathow, T. K. Eigentler, C. Garbe, K. Brechtel, R. Vonthein, R. Bares, C. D. Claussen, and H. P. Schlemmer, "Prospective comparison of 18F-fluorodeoxyglucose positron emission tomography/computed tomography and whole-body magnetic resonance imaging in staging of advanced malignant melanoma," Eur. J. Cancer **43**(3), 557–564 (2007).
[68]G. Schmidt, A. Haug, S. Schoenberg, and M. Reiser, "Whole-body MRI and PET-CT in the management of cancer patients," Eur. Radiol. **16**(6), 1216–1225 (2006).
[69]M. D. Seemann, "Whole-body PET/MRI: The future in oncological imaging," Technol. Cancer Res. Treat. **4**(5), 577–582 (2005).
[70]O. Ratib, J.-P. Willi, M. Wissmeyer, C. Steiner, M. Allaoua, V. Garibotto, O. Rager, H. Zaidi, M. Becker, J. P. Vallee, P. Loubeyre, and C. Becker, "Clinical application of whole body hybrid PET-MR scanner in oncology [abstract]," Eur. J. Nucl. Med. Mol. Imaging **37**(Suppl 2), S220 (2010).
[71]T. C. Kwee, T. Takahara, R. Ochiai, D. M. Koh, Y. Ohno, K. Nakanishi, T. Niwa, T. L. Chenevert, P. R. Luijten, and A. Alavi, "Complementary roles of whole-body diffusion-weighted MRI and 18F-FDG PET: The state of the art and potential applications," J. Nucl. Med. **51**(10), 1549–1558 (2010).
[72]T. A. Heusner, S. Hahn, C. Jonkmanns, S. Kuemmel, F. Otterbach, M. E. Hamami, A. R. Stahl, A. Bockisch, M. Forsting, and G. Antoch, "Diagnostic accuracy of fused positron emission tomography/magnetic resonance mammography: Initial results," Br. J. Radiol. **84**(998), 126–135 (2011).
[73]G. Delso and S. Ziegler, "PET/MRI system design," Eur. J. Nucl. Med. Mol. Imaging **36**(Suppl 1), 86–92 (2009).
[74]D. Gagnon, M. Morich, D. Blakely, and K. Nieman, "Hybrid PET/MR Imaging Systems," U. S. Patent Application Publication No. 2008/0312526 (2008).
[75]H. Zaidi, N. Ojha, M. Morich, J. Griesmer, Z. Hu, P. Maniawski, O. Ratib, D. Izquierdo-Garcia, Z. A. Fayad, and L. Shao, "Design and performance evaluation of a whole-body Ingenuity TF PET-MRI system," Phys. Med. Biol. **56**(10), 3091–3106 (2011).
[76]C. Catana, T. Benner, A. van der Kouwe, L. Byars, M. Hamm, D. B. Chonde, C. J. Michel, G. El Fakhri, M. Schmand, and A. G. Sorensen, "MRI-assisted PET motion correction for neurologic studies in an integrated MR-PET scanner," J. Nucl. Med. **52**(1), 154–161 (2011).
[77]B. Lipinski, H. Herzog, E. Rota Kops, W. Oberschelp, and H. W. Muller-Gartner, "Expectation maximization reconstruction of positron emission tomography images using anatomical magnetic resonance information," IEEE Trans. Med. Imaging **16**(2), 129–136 (1997).
[78]K. Baete, J. Nuyts, W. Van Paesschen, P. Suetens, and P. Dupont, "Anatomical-based FDG-PET reconstruction for the detection of hypometabolic regions in epilepsy," IEEE Trans. Med. Imaging **23**(4), 510–519 (2004).
[79]H. Zaidi and A. Alavi, "Current trends in PET and combined (PET/CT and PET/MR) systems design," PET Clin. **2**(2), 109–123 (2007).
[80]M. Rafecas, B. Mosler, M. Dietz, M. Pogl, A. Stamatakis, D. P. McElroy, and S. I. Ziegler, "Use of a Monte Carlo-based probability matrix for 3-D iterative reconstruction of MADPET-II data," IEEE Trans. Nucl. Sci. **51**(5), 2597–2605 (2004).
[81]S. Moehrs, M. Defrise, N. Belcari, A. Del Guerra, A. Bartoli, S. Fabbri, and G. Zanetti, "Multi-ray-based system matrix generation for 3D PET reconstruction," Phys. Med. Biol. **53**(23), 6925–6945 (2008).
[82]K. Yang, C. L. Melcher, P. D. Rack, and L. A. Eriksson, "Effects of calcium codoping on charge traps in LSO:Ce crystals," IEEE Trans. Nucl. Sci. **56**(5), 2960–2965 (2009).
[83]J. S. Karp, S. Surti, M. E. Daube-Witherspoon, and G. Muehllehner, "Benefit of time-of-flight in PET: Experimental and clinical results," J. Nucl. Med. **49**(3), 462–470 (2008).
[84]M. Conti, "State of the art and challenges of time-of-flight PET," Phys. Med. **25**(15), 1–11 (2009).
[85]M. Conti, "Focus on time-of-flight PET: The benefits of improved time resolution," Eur. J. Nucl. Med. Mol. Imaging **38**(6), 1147–1157 (2011).
[86]C. Lois, B. W. Jakoby, M. J. Long, K. F. Hubner, D. W. Barker, M. E. Casey, M. Conti, V. Y. Panin, D. J. Kadrmas, and D. W. Townsend, "An assessment of the impact of incorporating time-of-flight information into clinical PET/CT imaging," J. Nucl. Med. **51**(2), 237–245 (2010).
[87]G. El Fakhri, S. Surti, C. M. Trott, J. Scheuermann, and J. S. Karp, "Improvement in lesion detection with whole-body oncologic time-of-flight PET," J. Nucl. Med. **52**(3), 347–353 (2011).
[88]W. W. Moses, "Time of flight in PET revisited," IEEE Trans. Nucl. Sci. **50**(5), 1325–1330 (2003).
[89]Z. H. Cho, Y. D. Son, H. K. Kim, K. N. Kim, S. H. Oh, J. Y. Han, I. K. Hong, and Y. B. Kim, "A hybrid PET-MRI: An integrated molecular-genetic imaging system with HRRT-PET and 7.0-T MRI," Int. J. Imaging Syst. Technol. **17**(4), 252–265 (2007).
[90]U. Klose, "In vivo proton spectroscopy in presence of eddy currents," Magn. Reson. Med. **14**(1), 26–30 (1990).
[91]C. R. Camacho, D. B. Plewes, and R. M. Henkelman, "Nonsusceptibility artifacts due to metallic objects in MR imaging," J. Magn. Reson. Imaging **5**(1), 75–88 (1995).
[92]S. Furst, G. Delso, A. Martinez-Moller, B. Jakoby, F. Schoenahl, C. Ganter, S. Nekolla, S. Ziegler, E. Rummeny, and M. Schwaiger, "Initial performance evaluation of the Biograph mMR," J. Nucl. Med. **52**, 320 (2011).
[93]B. Pichler, E. Lorenz, R. Mirzoyan, W. Pimpl, F. Roder, and M. Schwaiger, "Performance tests of a LSO-APD PET module in a 9.4 Tesla magnet," *IEEE Nuclear Science Symposium and Medical Imaging Conference Record*, pp. 1237–1239 (1997).
[94]P. K. Marsden, D. Strul, S. F. Keevil, S. C. Williams, and D. Cash, "Simultaneous PET and NMR," Br. J. Radiol. **75 Spec No**, S53–S59 (2002).
[95]S. R. Cherry, "Multimodality in vivo imaging systems: Twice the power or double the trouble?," Annu. Rev. Biomed. Eng. **8**, 35–62 (2006).
[96]S. R. Cherry, A. Y. Louie, and R. E. Jacobs, "The integration of positron emission tomography with magnetic resonance imaging," Proc. IEEE **96**(3), 416–438 (2008).
[97]D. Schlyer, P. Vaska, D. Tomasi, C. Woody, W. Rooney, S. Maramraju, S. Southekal, J.-F. Pratte, S. Junnarkar, M. Purschke, S. Krishnamoorthy, A. Kriplani, and S. Stoll, "A simultaneous PET/MRI scanner based on the RatCAP," *IEEE Nuclear Science Symposium Conference Record*, pp. 3256–3259 (2007).
[98]J. Kang, Y. Choi, K. J. Hong, J. H. Jung, W. Hu, Y. S. Huh, H. Lim, and B.-T. Kim, "A feasibility study of photosensor charge signal transmission to preamplifier using long cable for development of hybrid PET-MRI," Med. Phys. **37**(11), 5655–5664 (2010).
[99]Y. Wu, C. Catana, R. Farrell, P. A. Dokhale, K. S. Shah, Q. Jinyi, and S. R. Cherry, "PET performance evaluation of an MR-compatible PET insert," IEEE Trans. Nucl. Sci. **56**(3), 574–580 (2009).
[100]H. F. Wehrl, M. S. Judenhofer, A. Thielscher, P. Martirosian, F. Schick, and B. J. Pichler, "Assessment of MR compatibility of a PET insert developed for simultaneous multiparametric PET/MR imaging on an animal system operating at 7 T," Magn. Reson. Med. **65**(1), 269–279 (2010).
[101]H. Wehrl, M. Judenhofer, S. Wiehr, and B. Pichler, "Pre-clinical PET/MR: Technological advances and new perspectives in biomedical research," Eur. J. Nucl. Med. Mol. Imaging **36**(Suppl 1), 56–68 (2009).

[102]R. Fontaine, F. Belanger, N. Viscogliosi, H. Semmaoui, M. A. Tetrault, J. B. Michaud, C. Pepin, J. Cadorette, and R. Lecomte, "The hardware and signal processing architecture of LabPET^{TM}, a small animal APD-based digital PET scanner," IEEE Trans. Nucl. Sci. **56**(1), 3–9 (2009).
[103]A. N. Otte, J. Barral, B. Dolgoshein, J. Hose, S. Klemin, E. Lorenz, R. Mirzoyan, E. Popova, and M. Teshima, "A test of silicon photomultipliers as readout for PET," Nucl. Instrum. Methods Phys. Res. A **545**(3), 705–715 (2005).
[104]P. Buzhan, B. Dolgoshein, A. Ilyin, V. Kantserov, V. Kaplin, A. Karakash, A. Pleshko, E. Popova, S. Smirnov, Y. Volkov, L. Filatov, S. Klemin, and F. Kayumov, "An advanced study of silicon photomultiplier," ICFA Instrum. Bull. **23**, 28–42 (2001).
[105]D. J. Herbert, V. Saveliev, N. Belcari, N. D'Ascenzo, A. Del Guerra, and A. Golovin, "First results of scintillator readout with silicon photomultiplier," IEEE Trans. Nucl. Sci. **53**(1), 389–394 (2006).
[106]C. Piemonte, R. Battiston, M. Boscardin, G. Collazuol, F. Corsi, G. F. Dalla Betta, A. Del Guerra, N. Dinu, G. Levi, G. Llosa, S. Marcatili, C. Marzocca, A. Pozza, and N. Zorzi, "New results on the characterization of ITC-irst silicon photomultipliers," *IEEE Nuclear Science Symposium Conference Record*, pp. 1566–1569 (2006).
[107]G. Llosa, N. Belcari, M. G. Bisogni, G. Collazuol, A. Del Guerra, S. Marcatili, S. Moehrs, and C. Piemonte, "Silicon photomultipliers and SiPM matrices as photodetectors in nuclear medicine," *IEEE Nuclear Science Symposium Conference Record*, pp. 3220–3223 (2007).
[108]R. Hawkes, A. Lucas, J. Stevick, G. Llosa, S. Marcatili, C. Piemonte, A. Del Guerra, and T. A. Carpenter, "Silicon photomultiplier performance tests in magnetic resonance pulsed fields," *IEEE Nuclear Science Symposium Conference Record*, pp. 3400–3403 (2007).
[109]C. Piemonte, B. Roberto, B. Maurizio, B. Gian-Franco Dalla, G. Alberto Del, D. Nicoleta, P. Alberto, and Z. Nicola, "Characterization of the first prototypes of silicon photomultiplier fabricated at ITC-irst," IEEE Trans. Nucl. Sci. **54**(1), 236–244 (2007).
[110]G. Llosa, R. Battiston, N. Belcari, M. Boscardin, G. Collazuol, F. Corsi, G.-F. Dalla Betta, A. Del Guerra, N. Dinu, G. Levi, S. Marcatili, S. Moehrs, C. Marzocca, C. Piemonte, and A. Pozza, "Novel silicon photomultipliers for PET applications," IEEE Trans. Nucl. Sci. **55**(3), 877–881 (2008).
[111]N. Dinu, P. Barrillon, C. Bazin, N. Belcari, M. G. Bisogni, S. Bondil-Blin, M. Boscardin, V. Chaumat, G. Collazuol, C. De La Taille, A. Del Guerra, G. Llosá, S. Marcatili, M. Melchiorri, C. Piemonte, V. Puill, A. Tarolli, J. F. Vagnucci, and N. Zorzi, "Characterization of a prototype matrix of silicon photomultipliers," Nucl. Instrum. Methods Phys. Res. A **610**(1), 101–104 (2009).
[112]G. Collazuol, G. Ambrosi, M. Boscardin, F. Corsi, G. F. Dalla Betta, A. Del Guerra, M. Galimberti, D. Giulietti, L. A. Gizzi, L. Labate, G. Llosa, S. Marcatili, C. Piemonte, A. Pozza, and N. Zorzi, "Single timing resolution and detection efficiency of the ITC-irst silicon photomultipliers," Nucl. Instrum. Methods Phys. Res. A **581**, 461–464 (2007).
[113]P. Barrillon, S. Blin, M. Bouchel, T. Caceres, C. de La Taille, G. Martin, P. Puzo, and N. Seguin-Moreau, "MAROC: Multi-anode readout chip for MaPMTs," *IEEE Nuclear Science Symposium Conference Record*, pp. 809–814 (2006).
[114]G. Llosá, N. Belcari, M. G. Bisogni, G. Collazuol, S. Marcatili, M. Boscardin, M. Melchiorri, A. Tarolli, C. Piemonte, N. Zorzi, P. Barrillon, S. Bondil-Blin, V. Chaumat, C. de La Taille, N. Dinu, V. Puill, J. F. Vagnucci, and A. Del Guerra, "First results in the application of silicon photomultiplier matrices to small animal PET," Nucl. Instrum. Methods Phys. Res. A **610**(1), 196–199 (2009).
[115]M. Bouchel, S. Callier, F. Dulucq, J. Fleury, J.-J. Jaeger, C. de La Taille, G. Martin-Chassard, and L. Raux, "SPIROC (SiPM integrated read-out chip): Dedicated very front-end electronics for an ILC prototype hadronic calorimeter with SiPM read-out," J. Instrum. **6**(01), C01098 (2011).
[116]P. Fischer, I. Peric, M. Ritzert, and M. Koniczek, "Fast self triggered multi channel readout ASIC for time- and energy measurement," IEEE Trans. Nucl. Sci. **56**(3), 1153–1158 (2009).
[117]F. Corsi, A. Dragone, C. Marzocca, A. Del Guerra, P. Delizia, N. Dinu, C. Piemonte, M. Boscardin, and G. F. Dalla Betta, "Modelling a silicon photomultiplier (SiPM) as a signal source for optimum front-end design," Nucl. Instrum. Methods Phys. Res. A **572**(1), 416–418 (2007).
[118]F. Corsi, M. Foresta, C. Marzocca, G. Matarrese, and A. Del Guerra, "BASIC: An 8-channel front-end ASIC for silicon photomultiplier detectors," *IEEE Nuclear Science Symposium Conference Record (NSS/MIC)*, pp. 1082–1087 (2009).
[119]F. Corsi, A. G. Argentieri, M. Foresta, C. Marzocca, G. Matarrese, and A. Del Guerra, "Front-end electronics for silicon photomultipliers coupled to fast scintillators," *IEEE Nuclear Science Symposium Conference Record (NSS/MIC)*, pp. 1332–1339 (2010).
[120]S. Marcatili, N. Belcari, M. G. Bisogni, G. Collazuol, G. Ambrosi, F. Corsi, M. Foresta, C. Marzocca, G. Matarrese, G. Sportelli, P. Guerra, A. Santos, and A. Del Guerra, "Development and characterization of a modular acquisition system for a 4D PET block detector," Nucl. Instr. Meth. A (in press).
[121]G. Collazuol, M. G. Bisogni, S. Marcatili, C. Piemonte, and A. Del Guerra, "Studies of silicon photomultipliers at cryogenic temperatures," Nucl. Instrum. Methods Phys. Res. A **628**(1), 389–392 (2011).
[122]T. Solf, V. Schulz, B. Weissler, A. Thon, P. Fischer, M. Ritzert, V. Mlotok, C. Piemonte, and N. Zorzi, "Solid-state detector stack for ToF-PET/MR," *IEEE Nuclear Science Symposium Conference Record (NSS/MIC)*, pp. 2798–2799 (2009).
[123]www.hybrid-pet-mr.eu.
[124]www.sublimapet-mr.eu.
[125]A. Drzezga, M. Souvatzoglou, A. Beer, S. Ziegler, S. Furst, S. Nekolla, and M. Schwaiger, "Integrated simultaneous whole-body MR/PET: First comparison between MR/PET and PET/CT in patients," J. Nucl. Med. **52**, 262 (2011).
[126]S. Basu, H. Zaidi, M. Houseni, J. Udupa, P. Acton, D. Torigian, and A. Alavi, "Novel quantitative techniques for assessing regional and global function and structure based on modern imaging modalities: Implications for normal variation, aging and diseased states," Semin. Nucl. Med. **37**(3), 223–239 (2007).
[127]H. Zaidi, T. Ruest, F. Schoenahl, and M.-L. Montandon, "Comparative evaluation of statistical brain MR image segmentation algorithms and their impact on partial volume effect correction in PET," Neuroimage **32**(4), 1591–1607 (2006).
[128]H. Zaidi and B. H. Hasegawa, "Determination of the attenuation map in emission tomography," J. Nucl. Med. **44**(2), 291–315 (2003).
[129]P. E. Kinahan, B. H. Hasegawa, and T. Beyer, "X-ray-based attenuation correction for positron emission tomography/computed tomography scanners," Semin. Nucl. Med. **33**(3), 166–179 (2003).
[130]H. Zaidi, "Is MRI-guided attenuation correction a viable option for dual-modality PET/MR imaging?," Radiology **244**(3), 639–642 (2007).
[131]M. Hofmann, B. Pichler, B. Schölkopf, and T. Beyer, "Towards quantitative PET/MRI: A review of MR-based attenuation correction techniques," Eur. J. Nucl. Med. Mol. Imaging **36**(Suppl 1), 93–104 (2009).
[132]H. Zaidi, "Is radionuclide transmission scanning obsolete for dual-modality PET/CT systems?," Eur. J. Nucl. Med. Mol. Imaging **34**(6), 815–818 (2007).
[133]H. Zaidi, M.-L. Montandon, and A. Alavi, "Advances in attenuation correction techniques in PET," PET Clin. **2**(2), 191–217 (2007).
[134]H. Zaidi and K. F. Koral, "Scatter modelling and compensation in emission tomography," Eur. J. Nucl. Med. Mol. Imaging **31**(5), 761–782 (2004).
[135]C. C. Watson, "New, faster, image-based scatter correction for 3D PET," IEEE Trans. Nucl. Sci. **47**, 1587–1594 (2000).
[136]C. C. Watson, M. E. Casey, C. Michel, and B. Bendriem, "Advances in scatter correction for 3D PET/CT," *Nuclear Science Symposium Conference Record*, Oct. 19–22, Rome, Italy, pp. 3008–3012 (2004).
[137]S. D. Wollenweber, "Parameterization of a model-based 3-D PET scatter correction," IEEE Trans. Nucl. Sci. **49**(3), 722–727 (2002).
[138]R. Accorsi, L.-E. Adam, M. E. Werner, and J. S. Karp, "Optimization of a fully 3D single scatter simulation algorithm for 3D PET," Phys. Med. Biol. **49**(12), 2577–2598 (2004).
[139]C. S. Levin, M. Dahlbom, and E. J. Hoffman, "A Monte Carlo correction for the effect of Compton scattering in 3-D PET brain imaging," IEEE Trans. Nucl. Sci. **42**, 1181–1188 (1995).
[140]H. Zaidi, "Comparative evaluation of scatter correction techniques in 3D positron emission tomography," Eur. J. Nucl. Med. **27**(12), 1813–1826 (2000).
[141]C. H. Holdsworth, C. S. Levin, M. Janecek, M. Dahlbom, and E. J. Hoffman, "Performance analysis of an improved 3-D PET Monte Carlo simulation and scatter correction," IEEE Trans. Nucl. Sci. **49**(1), 83–89 (2002).
[142]J. Fripp, S. Crozier, S. K. Warfield, and S. Ourselin, "Automatic segmentation of the bone and extraction of the bone–cartilage interface from magnetic resonance images of the knee," Phys. Med. Biol. **52**(6), 1617–1631 (2007).

[143]J. Fripp, S. Crozier, S. K. Warfield, and S. Ourselin, "Automatic segmentation and quantitative analysis of the articular cartilages from magnetic resonance images of the knee," IEEE Trans. Med. Imaging **29**(1), 55–64 (2010).
[144]A. Martinez-Moller, M. Souvatzoglou, G. Delso, R. A. Bundschuh, C. Chefd'hotel, S. I. Ziegler, N. Navab, M. Schwaiger, and S. G. Nekolla, "Tissue classification as a potential approach for attenuation correction in whole-body PET/MRI: Evaluation with PET/CT data," J. Nucl. Med. **50**(4), 520–526 (2009).
[145]Z. Hu, N. Ojha, S. Renisch, V. Schulz, I. Torres, D. Pal, G. Muswick, J. Penatzer, T. Guo, P. Boernert, C.-H. Tung, J. Kaste, L. Shao, M. Morich, T. Havens, P. Maniawski, W. Schaefer, R. Guenther, and G. Krombach, "MR-based attenuation correction for a whole-body sequential PET/MR system," *IEEE Nuclear Science Symposium and Medical Imaging Conference*, pp. 3508–3512 (2009).
[146]V. Schulz, I. Torres-Espallardo, S. Renisch, Z. Hu, N. Ojha, P. Börnert, M. Perkuhn, T. Niendorf, W. Schäfer, H. Brockmann, T. Krohn, A. Buhl, R. Günther, F. Mottaghy, and G. Krombach, "Automatic, three-segment, MR-based attenuation correction for whole-body PET/MR data," Eur. J. Nucl. Med. Mol. Imaging **38**(1), 138–152 (2011).
[147]J. Steinberg, G. Jia, S. Sammet, J. Zhang, N. Hall, and M. V. Knopp, "Three-region MRI-based whole-body attenuation correction for automated PET reconstruction," Nucl. Med. Biol. **37**(2), 227–235 (2010).
[148]H. Zaidi, M.-L. Montandon, and D. O. Slosman, "Magnetic resonance imaging-guided attenuation and scatter corrections in three-dimensional brain positron emission tomography," Med. Phys. **30**(5), 937–948 (2003).
[149]H. Zaidi, M.-L. Montandon, and S. Meikle, "Strategies for attenuation compensation in neurological PET studies," Neuroimage **34**(2), 518–541 (2007).
[150]E. Rota Kops and H. Herzog, "Alternative methods for attenuation correction for PET images in MR-PET scanners," *Proceedings of the IEEE Nuclear Science Symposium and Medical Imaging Conference*, pp. 4327–4330 (2007).
[151]B. Dogdas, D. W. Shattuck, and R. M. Leahy, "Segmentation of skull and scalp in 3-D human MRI using mathematical morphology," Hum. Brain Mapp. **26**(4), 273–285 (2005).
[152]V. Keereman, Y. Fierens, T. Broux, Y. De Deene, M. Lonneux, and S. Vandenberghe, "MRI-based attenuation correction for PET/MRI using ultrashort echo time sequences," J. Nucl. Med. **51**(5), 812–818 (2010).
[153]C. Catana, A. van der Kouwe, T. Benner, C. J. Michel, M. Hamm, M. Fenchel, B. Fischl, B. Rosen, M. Schmand, and A. G. Sorensen, "Toward implementing an MRI-based PET attenuation-correction method for neurologic studies on the MR-PET brain prototype," J. Nucl. Med. **51**(9), 1431–1438 (2010).
[154]Z. Hu, S. Renisch, B. Schweizer, T. Blaffert, N. Ojha, T. Guo, J. Tang, C.-H. Tung, J. Kaste, V. Schulz, I. Torres, and L. Shao, "MR-based attenuation correction for a whole-body PET/MR system," *IEEE Nuclear Science Symposium and Medical Imaging Conference*, pp. 2119–2122 (2010).
[155]P. J. Robinson and L. Kreel, "Pulmonary tissue attenuation with computed tomography: Comparison of inspiration and expiration scans," J. Comput. Assist. Tomogr. **3**(6), 740–748 (1979).
[156]M.-L. Montandon and H. Zaidi, "Atlas-guided non-uniform attenuation correction in cerebral 3D PET imaging," Neuroimage **25**(1), 278–286 (2005).
[157]E. Schreibmann, J. A. Nye, D. M. Schuster, D. R. Martin, J. Votaw, and T. Fox, "MR-based attenuation correction for hybrid PET-MR brain imaging systems using deformable image registration," Med. Phys. **37**(5), 2101–2109 (2010).
[158]M. Hofmann, F. Steinke, V. Scheel, G. Charpiat, J. Farquhar, P. Aschoff, M. Brady, B. Scholkopf, and B. J. Pichler, "MRI-based attenuation correction for PET/MRI: A novel approach combining pattern recognition and Atlas registration," J. Nucl. Med. **49**(11), 1875–1883 (2008).
[159]S. Klein, M. Staring, K. Murphy, M. A. Viergever, and J. P. W. Pluim, "Elastix: A toolbox for intensity-based medical image registration," IEEE Trans. Med. Imaging **29**(1), 196–205 (2010).
[160]B. Zhang, D. Pal, Z. Hu, N. Ojha, G. Muswick, C.-H. Tung, and J. Kaste, "Attenuation correction for MR table and coils for a sequential PET/MR system," *IEEE Nuclear Science Symposium and Medical Imaging Conference*, pp. 3303–3306 (2009).
[161]G. Delso, A. Martinez-Moller, R. A. Bundschuh, R. Ladebeck, Y. Candidus, D. Faul, and S. I. Ziegler, "Evaluation of the attenuation properties of MR equipment for its use in a whole-body PET/MR scanner," Phys. Med. Biol. **55**(15), 4361–4374 (2010).
[162]F. Mantlik, M. Hofmann, M. K. Werner, A. Sauter, J. Kupferschlager, B. Scholkopf, B. J. Pichler, and T. Beyer, "The effect of patient positioning aids on PET quantification in PET/MR imaging," Eur. J. Nucl. Med. Mol. Imaging **38**(5), 920–929 (2011).
[163]G. Delso, A. Martinez-Moller, R. A. Bundschuh, S. G. Nekolla, and S. I. Ziegler, "The effect of limited MR field of view in MR/PET attenuation correction," Med. Phys. **37**(6), 2804–2812 (2010).
[164]J. Nuyts, C. Michel, M. Fenchel, G. Bal, and C. C. Watson, "Completion of a truncated attenuation image from the attenuated PET emission data," *IEEE Nuclear Science Symposium and Medical Imaging Conference*, pp. 2123–2127 (2010).
[165]T. G. Turkington and J. M. Wilson, "Attenuation artifacts and time-of-flight PET," *IEEE Nuclear Science Symposium Conference Record (NSS/MIC)*, pp. 2997–2999 (2009).
[166]A. Salomon, A. Goedicke, B. Schweizer, T. Aach, and V. Schulz, "Simultaneous reconstruction of activity and attenuation for PET/MR," IEEE Trans. Med. Imaging **30**(3), 804–813 (2011).
[167]A. J. Reader and H. Zaidi, "Advances in PET image reconstruction," PET Clin. **2**(2), 173–190 (2007).
[168]P. J. Green, "Bayesian reconstructions from emission tomography data using a modified EM algorithm," IEEE Trans. Med. Imaging **9**(1), 84–93 (1990).
[169]C. Comtat, P. E. Kinahan, J. A. Fessler, T. Beyer, D. W. Townsend, M. Defrise, and C. Michel, "Clinically feasible reconstruction of 3D whole-body PET/CT data using blurred anatomical labels," Phys. Med. Biol. **47**(1), 1–20 (2002).
[170]G. Gindi, M. Lee, A. Rangarajan, and I. G. Zubal, "Bayesian reconstruction of functional images using anatomical information as priors," IEEE Trans. Med. Imaging **12**(4), 670–680 (1993).
[171]J. Tang and A. Rahmim, "Bayesian PET image reconstruction incorporating anato-functional joint entropy," Phys. Med. Biol. **54**(23), 7063–7075 (2009).
[172]M. Soret, S. L. Bacharach, and I. Buvat, "Partial-volume effect in PET tumor imaging," J. Nucl. Med. **48**(6), 932–945 (2007).
[173]R. M. Kessler, J. R. Ellis, and M. Eden, "Analysis of emission tomographic scan data: Limitations imposed by resolution and background," J. Comput. Assist. Tomogr. **8**(3), 514–522 (1984).
[174]L. Geworski, B. O. Knoop, M. L. de Cabrejas, W. H. Knapp, and D. L. Munz, "Recovery correction for quantitation in emission tomography: A feasibility study," Eur. J. Nucl. Med. **27**(2), 161–169 (2000).
[175]M. Quarantelli, K. Berkouk, A. Prinster, B. Landeau, C. Svarer, L. Balkay, B. Alfano, A. Brunetti, J.-C. Baron, and M. Salvatore, "Integrated software for the analysis of brain PET/SPECT studies with partial-volume-effect correction," J. Nucl. Med. **45**(2), 192–201 (2004).
[176]A. J. Da Silva, H. R. Tang, K. H. Wong, M. C. Wu, M. W. Dae, and B. H. Hasegawa, "Absolute quantification of regional myocardial uptake of 99mTc-sestamibi with SPECT: Experimental validation in a porcine model," J. Nucl. Med. **42**, 772–779 (2001).
[177]H. Matsuda, T. Ohnishi, T. Asada, Z. J. Li, H. Kanetaka, E. Imabayashi, F. Tanaka, and S. Nakano, "Correction for partial-volume effects on brain perfusion SPECT in healthy men," J. Nucl. Med. **44**(8), 1243–1252 (2003).
[178]M. Shidahara, C. Tsoumpas, A. Hammers, N. Boussion, D. Visvikis, T. Suhara, I. Kanno, and F. E. Turkheimer, "Functional and structural synergy for resolution recovery and partial volume correction in brain PET," Neuroimage **44**(2), 340–348 (2009).
[179]K. Baete, J. Nuyts, K. V. Laere, W. Van Paesschen, S. Ceyssens, L. De Ceuninck, O. Gheysens, A. Kelles, J. Van den Eynden, P. Suetens, and P. Dupont, "Evaluation of anatomy based reconstruction for partial volume correction in brain FDG-PET," Neuroimage **23**(1), 305–317 (2004).
[180]A. Rahmim, O. Rousset, and H. Zaidi, "Strategies for motion tracking and correction in PET," PET Clin. **2**(2), 251–266 (2007).
[181]A. J. van der Kouwe, T. Benner, and A. M. Dale, "Real-time rigid body motion correction and shimming using cloverleaf navigators," Magn. Reson. Med. **56**(5), 1019–1032 (2006).
[182]C. Tsoumpas, J. E. Mackewn, P. Halsted, A. P. King, C. Buerger, J. J. Totman, T. Schaeffter, and P. K. Marsden, "Simultaneous PET-MR acquisition and MR-derived motion fields for correction of non-rigid motion in PET," Ann. Nucl. Med. **24**(10), 745–750 (2010).
[183]P. Kellman, C. Chefd'hotel, C. H. Lorenz, C. Mancini, A. E. Arai, and E. R. McVeigh, "Fully automatic, retrospective enhancement of real-time acquired cardiac cine MR images using image-based navigators and respiratory motion-corrected averaging," Magn. Reson. Med. **59**(4), 771–778 (2008).

[184]A. H. Davarpanah, Y. P. Chen, A. Kino, C. T. Farrelly, A. N. Keeling, J. J. Sheehan, A. B. Ragin, P. J. Weale, S. Zuehlsdorff, and J. C. Carr, "Accelerated two- and three-dimensional cine MR imaging of the heart by using a 32-channel coil," Radiology **254**(1), 98–108 (2010).
[185]J. Czernin, M. Allen-Auerbach, and H. R. Schelbert, "Improvements in cancer staging with PET/CT: Literature-based evidence as of September 2006," J. Nucl. Med. **48** (Suppl 1), 78S–88S (2007).
[186]M. F. Di Carli, S. Dorbala, J. Meserve, G. El Fakhri, A. Sitek, and S. C. Moore, "Clinical myocardial perfusion PET/CT," J. Nucl. Med. **48**(5), 783–793 (2007).
[187]P. A. Kaufmann and M. F. Di Carli, "Hybrid SPECT/CT and PET/CT imaging: The next step in noninvasive cardiac imaging," Semin. Nucl. Med. **39**(5), 341–347 (2009).
[188]D. C. Costa, L. S. Pilowsky, and P. J. Ell, "Nuclear medicine in neurology and psychiatry," Lancet **354**(9184), 1107–1111 (1999).
[189]K. Tatsch and P. J. Ell, "PET and SPECT in common neuropsychiatric disease," Clin. Med. **6**(3), 259–262 (2006).
[190]H.-J. Wester, "Nuclear imaging probes: From bench to bedside," Clin. Cancer Res. **13**(12), 3470–3481 (2007).
[191]C. A. Pelizzari, G. T. Chen, D. R. Spelbring, R. R. Weichselbaum, and C. T. Chen, "Accurate three-dimensional registration of CT, PET, and/or MR images of the brain," J. Comput. Assist. Tomogr. **13**(1), 20–26 (1989).
[192]R. P. Woods, J. C. Mazziotta, and S. R. Cherry, "MRI-PET registration with automated algorithm," J. Comput. Assist. Tomogr. **17**(4), 536–546 (1993).
[193]S. Gilman, "Imaging the brain. First of two parts," N. Engl. J. Med. **338**(12), 812–820 (1998).
[194]K. Goffin, S. Dedeurwaerdere, K. Van Laere, and W. Van Paesschen, "Neuronuclear assessment of patients with epilepsy," Semin. Nucl. Med. **38**(4), 227–239 (2008).
[195]W. Chen and D. H. S. Silverman, "Advances in evaluation of primary brain tumors," Semin. Nucl. Med. **38**(4), 240–250 (2008).
[196]H. Vees, S. Senthamizhchelvan, R. Miralbell, D. Weber, O. Ratib, and H. Zaidi, "Assessment of various strategies for 18F-FET PET-guided delineation of target volumes in high-grade glioma patients," Eur. J. Nucl. Med. Mol. Imaging **36**(2), 182–193 (2009).
[197]S. Bisdas, T. Nagele, H. P. Schlemmer, A. Boss, C. D. Claussen, B. Pichler, and U. Ernemann, "Switching on the lights for real-time multimodality tumor neuroimaging: The integrated positron–emission tomography/MR imaging system," AJNR Am. J. Neuroradiol. **31**(4), 610–614 (2010).
[198]A. Boss, S. Bisdas, A. Kolb, M. Hofmann, U. Ernemann, C. D. Claussen, C. Pfannenberg, B. J. Pichler, M. Reimold, and L. Stegger, "Hybrid PET/MRI of intracranial masses: Initial experiences and comparison to PET/CT," J. Nucl. Med. **51**(8), 1198–1205 (2010).
[199]D. Thorwarth, G. Henke, A. C. Muller, M. Reimold, T. Beyer, A. Boss, A. Kolb, B. Pichler, and C. Pfannenberg, "Simultaneous (68)Ga-DOTA-TOC-PET/MRI for IMRT treatment planning for meningioma: First experience," Int. J. Radiat. Oncol., Biol., Phys. **81**(1), 277–283 (2011).
[200]A. Boss, L. Stegger, S. Bisdas, A. Kolb, N. Schwenzer, M. Pfister, C. D. Claussen, B. J. Pichler, and C. Pfannenberg, "Feasibility of simultaneous PET/MR imaging in the head and upper neck area," Eur. Radiol. **21**(7), 1439–1446 (2011).
[201]Z. H. Cho, Y. D. Son, H. K. Kim, N. B. Kim, E. J. Choi, S. Y. Lee, J. G. Chi, C. W. Park, Y. B. Kim, and S. Ogawa, "Observation of glucose metabolism in the thalamic nuclei by fusion PET/MRI," J. Nucl. Med. **52**(3), 401–414 (2011).
[202]D. Patel, A. Kell, B. Simard, B. Xiang, H. Y. Lin, and G. Tian, "The cell labeling efficacy, cytotoxicity and relaxivity of copper-activated MRI/PET imaging contrast agents," Biomaterials **32**(4), 1167–1176 (2011).
[203]D. Wagenaar, O. Nalcioglu, L. Muftuler, D. Meier, K. Parnham, M. Szawlowski, M. Kapusta, S. Azman, J. Gjaerum, G. Maehlum, Y. Wang, B. Tsui, and B. Patt, "A multi-ring small animal CZT system for simultaneous SPECT/MRI imaging," J. Nucl. Med. **48**, 89P (2007).
[204]M. J. Hamamura, S. Ha, W. W. Roeck, L. T. Muftuler, D. J. Wagenaar, D. Meier, B. E. Patt, and O. Nalcioglu, "Development of an MR-compatible SPECT system (MRSPECT) for simultaneous data acquisition," Phys. Med. Biol. **55**(6), 1563–1575 (2010).
[205]K. S. Lee, W. W. Roeck, G. T. Gullberg, and O. Nalcioglu, "MR-based keyhole SPECT for small animal imaging," Phys. Med. Biol. **56**(3), 685–702 (2011).
[206]www.medsum.info.
[207]G. Llosa, J. Barrio, C. Lacasta, M. G. Bisogni, A. Del Guerra, S. Marcatili, P. Barrillon, S. Bondil-Blin, C. de la Taille, and C. Piemonte, "Characterization of a PET detector head based on continuous LYSO crystals and monolithic, 64-pixel silicon photomultiplier matrices," Phys. Med. Biol. **55**(23), 7299–7315 (2010).